

Article

# Tuning Rules for Active Disturbance Rejection Controllers via Multiobjective Optimization—A Guide for Parameters Computation Based on Robustness

Blanca Viviana Martínez <sup>\*</sup>, Javier Sanchis , Sergio García-Nieto  and Miguel Martínez 

Instituto Universitario de Automática e Informática Industrial, Universitat Politècnica de València, 46022 Valencia, Spain; jsanchis@isa.upv.es (J.S.); sgnieto@isa.upv.es (S.G.-N.); mmiranzo@isa.upv.es (M.M.)

\* Correspondence: blamarca@doctor.upv.es

**Abstract:** A set of tuning rules for Linear Active Disturbance Rejection Controller (LADRC) with three different levels of compromise between disturbance rejection and robustness is presented. The tuning rules are the result of a Multiobjective Optimization Design (MOOD) procedure followed by curve fitting and are intended as a tool for designers who seek to implement LADRC by considering the load disturbance response of processes whose behavior is approximated by a general first-order system with delay. The validation of the proposed tuning rules is done through illustrative examples and the control of a nonlinear thermal process. Compared to classical PID (Proportional-Integral-Derivative) and other LADRC tuning methods, the derived functions offer an improvement in either disturbance rejection, robustness or both design objectives.

**Keywords:** active disturbance rejection control (ADRC); multiobjective optimization; time delay systems; tuning rules



**Citation:** Martínez, B. V.; Sanchis, J.; García-Nieto, S.; Martínez, M. Tuning Rules for Active Disturbance Rejection Controllers via Multiobjective Optimization: A Guide for Parameters Computation Based on Robustness. *Mathematics* **2021**, *9*, 517. <https://doi.org/10.3390/math9050517>

Academic Editors: Eva H. Dulf and Cristina I. Muresan

Received: 27 January 2021  
Accepted: 23 February 2021  
Published: 2 March 2021

**Publisher's Note:** MDPI stays neutral with regard to jurisdictional claims in published maps and institutional affiliations.



**Copyright:** © 2020 by the authors. Licensee MDPI, Basel, Switzerland. This article is an open access article distributed under the terms and conditions of the Creative Commons Attribution (CC BY) license (<https://creativecommons.org/licenses/by/4.0/>).

## 1. Introduction

Active Disturbance Rejection Control (ADRC) [1] was proposed as an alternative for PID (Proportional-Integral-Derivative) control and has become a new control paradigm. It inherits from the PID controller its independence from the plant model and seeks to compensate its weaknesses through the concept of disturbance estimation and rejection.

The ADRC lumps together the non-modeled dynamics and non-manipulable external signals affecting the system in a single total perturbation. This signal is treated as an extended state to be estimated by an Extended State Observer (ESO) and its impact on the output is rejected by the control action. As a result, the ADRC loop induces the real plant to behave like a set of cascade integrators facilitating the control design.

The fact that the extended observer jointly treats external perturbations and modeling uncertainties highlights its attractiveness in the engineering field, since the knowledge of the process model is kept to minimum in order to design the control loop. What is more, in contrast with model-based approaches, the ADRC assumes a canonical form regardless of the process dynamics and unifies the unknown discrepancies between the canonical form and the real plant in the total perturbation [2]. The effectiveness of the ADRC has been tested in a variety of fields including power electronics, motion and process control. A summary of recent experimental studies in the aforementioned areas can be found in [3]. The emergence of innovative ADRC solutions, particularly in industrial control, is a motivation to consider this control approach for processes where a precise dynamic model is difficult to obtain and a simplified approximation could be used instead.

The implementation of the ADRC requires the order of the system and the nominal value of its critical gain; being the latter the parameter that usually relates the control input with the highest order derivative of the output. When the ESO and the control law are designed by evaluation of nonlinear functions, the algorithm is called NADRC (Nonlinear

ADRC). On the other hand, if a linear observer together with a linear control law are used, the control strategy is called LADRC (Linear ADRC).

The LADRC has gained popularity due to its simple structure and the reduced amount of parameters to be tuned in comparison with the NADRC. The bandwidth parameterization [4] formulates the observer and control law gains as functions of two main parameters—the observer bandwidth and the controller bandwidth. Usually, their selection is based on the closed loop desired behavior and is adjusted by trial and error turning the tuning problem into an empirical process.

The tuning of the LADRC is considered a research area of interest. It has been addressed taking as a starting point PID controllers operating in the control system [5,6] or strictly proper controllers with integrator [7], which state the desired disturbance rejection performance.

The inclusion of the nominal value of the process critical gain as the third tuning parameter (in addition to the two bandwidths) has been discussed in [8,9]. In [10], the nominal value of the critical gain is tuned through an online optimization process for a tank level control problem. The main disadvantage of this approach is the time required to perform the optimization search on the loop.

To avoid the computational cost related to the online tuning, some researches have determined a set of functions to obtain the three main parameters (nominal value of critical gain, observer bandwidth and controller bandwidth). In [11] a tuning method for LADRC suitable for the control of a type of high-order systems is presented. It is based on the interpretation of the maximum sensitivity ( $M_S$ ) in the Nyquist diagram of the loop transfer function.

High-order plants can be used as approximations for some industrial processes. Nevertheless, the First Order Plus Dead Time (FOPDT) model is also a very common approximation which takes into account delays due to mass or energy transport, or limitations related to measuring and energy conversion devices [12]. The interest in the control of the FOPDT processes has inspired control strategies as the fractional order internal model controller (FO-IMC) from [13], where phase margin and gain crossover frequency specifications are employed to formulate a system of nonlinear equations which needs to be solved for the controller design.

On the other hand, tuning rules for the second order LADRC applied to FOPDT plants have been proposed in [14] through formulation of an optimization problem following the Aggregate Objective Function (AOF) approach. This is, two performance indices of interest as the settling time and the Integral of Squared Error (ISE) were merged in the Integral of Time Weighted Squared Error (ITSE) for minimization. In addition, a robustness measure was used as a fixed constraint.

The aforementioned work pointed out the importance of balancing the disturbance rejection performance with the closed loop robustness. However, including the robustness just as a constraint for the optimization problem could result in solutions offering an optimized performance (in terms of the index selected) but with a robustness measure that tends to be in the upper limit allowed. This may be enough for some designers, but for others, given the complexity of the process, robustness also becomes a design objective and a balance among all performance indices is required. As alternative, in the Generate-First Choose-Later (GFCL) multiobjective approach the objectives are optimized simultaneously providing a set of solutions, with different compromise, to be examined by the designer who makes the final decision.

Some contributions to the LADRC tuning have been made in the GFCL context. Nevertheless, they use the multiobjective approach to select some of the LADRC parameters to control a particular system or the optimization process needs to be performed for each design. For example, in [15] the Integral of Absolute Error (IAE) and the  $M_S$  are simultaneously minimized to select the LADRC bandwidths for the control of a power plant. In [16] a tuning scheme for the modified ADRC (MADRC) [17] for unstable time delay systems has been formulated as a multiobjective optimization problem regarding

the setpoint following and disturbance rejection. This methodology is intended to be performed adapting the problem according to the system to be controlled. It means that the proper MADRC order should be selected and the optimization and decision making stages need to be carried out for each study case in order to obtain the control law and observer gains.

Motivated by the above, this paper explores the GFCL approach to provide a set of tuning rules for the second-order LADRC parameters computation applicable to the control of FOPDT systems. A Multiobjective Optimization Design (MOOD) procedure is used over a group of nominal plants to obtain a set of Pareto optimal solutions with a compromise between the step load disturbance response and robustness. Then, the LADRC parameters are fitted to functions of the normalized delay and finally, these functions are scaled to make them suitable for the control of a general first order system with delay. Even though the LADRC has a certain level of robustness because it addresses the differences between the actual system and the assumed plant in the total perturbation, its tuning considering the robustness as an objective design balances this feature with the closed loop performance and this is reflected in the derived tuning rules.

The tuning rules presented here have prominent advantages for the control engineer:

- They can be used to control systems approximated by a FOPDT model because only the static gain, apparent time constant and apparent delay are required as prior information. The FOPDT is also known as the three-parameter model and is widely accepted in the control of industrial processes.
- The LADRC main parameters, this is, the nominal value of control gain, the controller bandwidth, and the observer bandwidth are automatically computed through the substitution of the model parameters in the given formulae.
- The designer can select a robustness quality (low, medium or high) for the parameters computation which allows his/her involvement as a decision maker, but eliminates the time and complexity of performing an entire optimization process for the controller design. This is possible because the robustness was included as a design objective in the optimization process formulation, in contrast with other approaches from literature where robustness is imposed just as a constraint, and also, different Pareto optimal solutions were used for the rules derivation.
- The parameters computed through the proposed rules ensure closed loop stability as well as a reasonable compromise between disturbance rejection and loop robustness.
- The designer could use the rules to obtain intervals for each LADRC parameter and adjust the selection according to the preferred performance. An LADRC tuning Matlab app (available at Matlab central [18]) was created for this purpose. Within this tool, the user can also vary the robustness level to visualize the performance with the corresponding calculated parameters.

The paper is organized as follows—in Section 2 the time domain and frequency domain formulation of the second-order LADRC as well as the loop parameterization are presented. In Section 3, a concise description of the Multiobjective Optimization Design procedure is given and the pertinence of this approach in the tuning of LADRC is addressed. Section 4 describes in detail the tuning of LADRC by means of the MOOD procedure whose results were fitted to the rules presented in Section 5. A summary guide for the LADRC parameters computation based on the proposed rules and the interactive tuning tool are also provided in this Section. Section 6 presents the validation of the proposal by the simulation of two examples. Performance comparison with classical PID tuning methods and the LADRC tuning rules from [11,14] are also presented. In Section 7 a nonlinear thermal process is controlled by the LADRC designed according to the proposed tuning method and, finally, Section 8 draws the conclusions.

## 2. Linear Active Disturbance Rejection Control

This section introduces the Linear Active Disturbance rejection control (LADRC) algorithm for single-input single-output systems.

The LADRC loop is mainly comprised of three blocks as shown in Figure 1.

- Tracking differentiator: It is used to generate a transient profile  $r_1$  for the reference  $\tilde{r}$  and the corresponding derivatives  $\dot{r}_1, \ddot{r}_1, \dots, r_1^{(n)}$ .
- Extended State Observer (ESO): It estimates the system states  $z_1, z_2, \dots, z_n$  and the additional state  $z_{n+1}$  representing the nonmodeled dynamics and perturbations.
- Controller: It provides a state feedback control law  $u_0$  for the disturbance-free modified plant. Therefore, the control law  $u = (u_0 - z_{n+1})/b_0$  is generated to act on the real plant and through which the disturbance information is rejected.

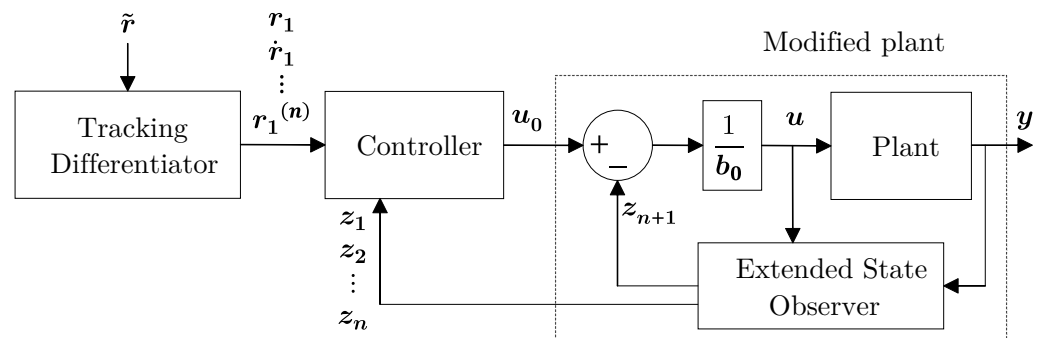


Figure 1. Active Disturbance Rejection Control (ADRC) loop.

For the LADRC implementation, the system order  $n$  and the nominal value of its critical gain  $b_0$  are required. Many practical applications can be approximated through first or second order models. Moreover, if the plant is open loop stable, a low order LADRC can be implemented and closed loop stability can be achieved by proper selection of the LADRC parameters [5].

In this work, the second-order LADRC was selected as control algorithm for FOPDT systems. The LADRC theoretical formulation in time domain and frequency domain, as well as the closed loop parameterization used for the development of the tuning rules are explained next.

### 2.1. Time Domain Formulation

Consider the following input-output model of a second order system.

$$\ddot{y} = -a_1\dot{y} - a_0y + bu, \tag{1}$$

where  $y$  is the controlled output,  $u$  is the control action,  $a_0$  and  $a_1$  are constants determining the location of the system poles and  $b$  is known as critical gain.

The state space representation of (1) is given by (2), where  $w$  has been included to indicate the load disturbances acting on the system.

$$\begin{cases} \dot{x}_1 = x_2 \\ \dot{x}_2 = -a_0x_1 - a_1x_2 + bu + w \\ y = x_1. \end{cases} \tag{2}$$

In the case that  $a_0$  and  $a_1$  are unknown, the first two terms in the right side of the expression for  $\dot{x}_2$  can be lumped in a function called total perturbation which also includes load disturbances and the difference between the real value of  $b$  and its known nominal value denoted by  $b_0$ . Thus,

$$f = -a_0x_1 - a_1x_2 + (b - b_0)u + w. \tag{3}$$

The model (4) is obtained by replacing (3) in (2).

$$\begin{cases} \dot{x}_1 = x_2 \\ \dot{x}_2 = f + b_0u \\ y = x_1. \end{cases} \tag{4}$$

As the total perturbation is an unknown function,  $f$  is treated as an additional state that must be estimated and compensated by the control loop. The resulting extended state space model with  $x_3 \triangleq f$  and  $h = \dot{f}$  unknown is

$$\begin{cases} \dot{x}_1 = x_2 \\ \dot{x}_2 = x_3 + b_0u \\ \dot{x}_3 = h \\ y = x_1. \end{cases} \tag{5}$$

The estimation of states in (5) is achieved through the Linear Extended State Observer (LESO) (6) whose inputs are the measured output  $y$  and the control action  $u$ . The  $z_i$  correspond to the estimated states and  $L_i$  are the observer gains. Note that, although the LESO has a similar structure to a traditional observer, it estimates not only the system states but also the information of the total perturbation contained in  $z_3$ . In contrast with the traditional observer, the LESO keeps the required amount of plant information to a minimum. The analysis of convergence and experimental validation of LESO are addressed in [19].

$$\begin{cases} \dot{z}_1 = z_2 + L_1(y - z_1) \\ \dot{z}_2 = z_3 + b_0u + L_2(y - z_1) \\ \dot{z}_3 = L_3(y - z_1). \end{cases} \tag{6}$$

According to Figure 1, the control law acting on the real plant is

$$u = \frac{u_0 - z_3}{b_0}. \tag{7}$$

Therefore, the double integrator (8) is obtained by replacing (7) in (4) and assuming that  $z_3 \approx f$ .

$$\begin{cases} \dot{x}_1 = x_2 \\ \dot{x}_2 = u_0 \\ y = x_1 \end{cases} \tag{8}$$

Equation (8) represents a disturbance-free modified plant which is controlled by the feedback law

$$u_0 = k_1(\tilde{r} - z_1) - k_2z_2, \tag{9}$$

where  $\tilde{r}$  is the setpoint and  $k_1$  and  $k_2$  are gains selected taking into account the desired closed loop performance. Note that  $\tilde{r}$  has been set as the reference in (9). This can be done in practice if the tracking differentiator is omitted or the setpoint derivatives are unbounded [20].

### 2.2. Frequency Domain Formulation

The block diagram from Figure 1 can be reformulated as the two degree-of-freedom configuration of Figure 2. The direct loop transfer function  $G_C(s)$  and the feedback transfer function  $G_F(s)$  are derived as follows.

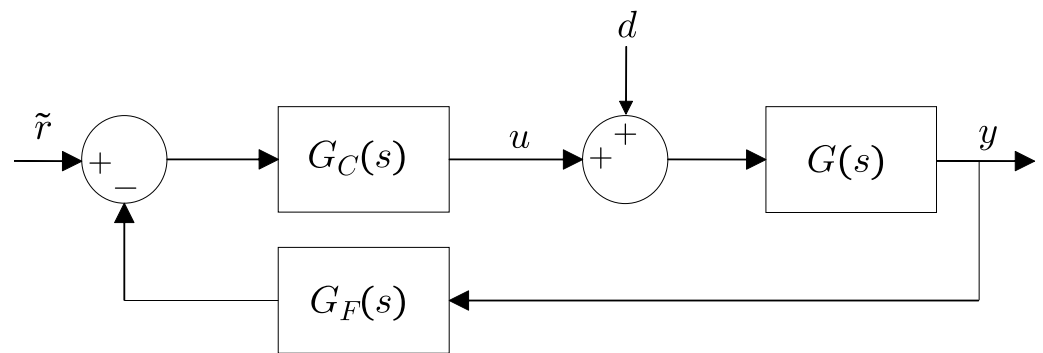


Figure 2. 2-degree-of-freedom (DOF) configuration of ADRC.

The linear extended state observer (6) in frequency domain is given by

$$\begin{cases} sZ_1 = Z_2 + L_1(Y - Z_1) \\ sZ_2 = Z_3 + b_0U + L_2(Y - Z_1) \\ sZ_3 = L_3(Y - Z_1), \end{cases} \tag{10}$$

where  $s$  is the complex variable,  $Y$  is the Laplace transform of the output,  $U$  is the Laplace transform of the control action and  $Z_i$  are the Laplace transforms of the states.

The expressions (11)–(13) are obtained by solving the system of Equation (10).

$$Z_1 = \frac{b_0s}{s^3 + L_1s^2 + L_2s + L_3}U + \frac{(L_1s^2 + L_2s + L_3)}{s^3 + L_1s^2 + L_2s + L_3}Y \tag{11}$$

$$Z_2 = \frac{b_0(s^2 + sL_1)}{s^3 + L_1s^2 + L_2s + L_3}U + \frac{(L_2s^2 + L_3s)}{s^3 + L_1s^2 + L_2s + L_3}Y \tag{12}$$

$$Z_3 = \frac{-L_3b_0}{s^3 + L_1s^2 + L_2s + L_3}U + \frac{L_3s^2}{s^3 + L_1s^2 + L_2s + L_3}Y. \tag{13}$$

The control action (14) is deduced by combining the frequency domain expressions of (7) and (9), with  $R$  being the Laplace transform of the reference.

$$U = \frac{1}{b_0}(k_1R - k_1Z_1 - k_2Z_2 - Z_3). \tag{14}$$

Therefore, substituting (11)–(13) in (14) and reorganizing terms,  $U$  is rewritten as

$$U = \frac{k_1}{b_0} \left[ \frac{s^3 + L_1s^2 + L_2s + L_3}{s^3 + (L_1 + k_2)s^2 + (k_2L_1 + L_2 + k_1)s} \right] R - \left[ \frac{(k_1L_1 + k_2L_2 + L_3)s^2 + (k_1L_2 + k_2L_3)s + k_1L_3}{b_0(s^3 + (L_1 + k_2)s^2 + (k_2L_1 + L_2 + k_1)s)} \right] Y. \tag{15}$$

From Figure 2 and in the absence of load disturbance ( $d = 0$ )

$$U = G_C(s)R - G_C(s)G_F(s)Y. \tag{16}$$

Hence, the resulting direct loop transfer function (17) and the feedback transfer function (18) are obtained comparing the factors of  $R$  and  $Y$  in (15) with those in (16).

$$G_C(s) = \frac{k_1}{b_0} \left( \frac{s^3 + L_1s^2 + L_2s + L_3}{s^3 + (L_1 + k_2)s^2 + (k_2L_1 + L_2 + k_1)s} \right) \tag{17}$$

$$G_F(s) = \frac{(k_1L_1 + k_2L_2 + L_3)s^2 + (k_2L_3 + k_1L_2)s + k_1L_3}{k_1(s^3 + L_1s^2 + L_2s + L_3)}. \tag{18}$$

Finally, the transfer function from output to load disturbance is

$$G_D(s) = \frac{G(s)}{1 + G(s)G_C(s)G_F(s)} \tag{19}$$

and the transfer function from control action to output is

$$G_U(s) = -G_C(s)G_F(s). \tag{20}$$

Equation (19) describes the system response to a load disturbance and (20) represents the LADRC transfer function for disturbance rejection.

### 2.3. Control Loop Parameterization

The control loop parameterization seeks a set of parameters that allows the computation of the complete set of LADRC gains. In addition, if an LADRC is designed for the control of a nominal system (e.g., a nominal FOPDT system), the loop parameterization also allows the parameters scaling in order to make the controller suitable for other systems of the same nature.

Consider the following theorem related to the scaling and bandwidth parameterization of the LADRC loop.

**Theorem 1.** [4] Assuming  $G_a(s)$  is a stabilizing controller for plant  $G_n(s)$  and the loop gain crossover frequency is  $\omega_c$ , then the controller

$$\bar{G}_a(s) = \frac{1}{k}G_a\left(\frac{s}{\omega_p}\right) \tag{21}$$

will stabilize the plant  $\bar{G}_n(s) = kG_n(s/\omega_p)$  and the new loop gain  $\bar{\mathcal{L}}(s) = \bar{G}_n(s)\bar{G}_a(s)$  will have a bandwidth of  $\omega_c\omega_p$ , and the same stability margins of  $\mathcal{L}(s) = G_n(s)G_a(s)$ .

In (21),  $k$  represents the gain scaling of plant  $kG_n(s)$  respect to  $G_n(s)$  and  $\omega_p$  is the frequency scaling of plant  $G_n(s/\omega_p)$  respect to  $G_n(s)$ .

Let  $G_A(s)$  be the transfer function obtained by multiplying  $G_C(s)$  and  $G_F(s)$  in the right hand side of (20). This is,

$$G_A(s) = \frac{(k_1L_1 + k_2L_2 + L_3)s^2 + (k_2L_3 + k_1L_2)s + k_1L_3}{b_0(s^3 + (L_1 + k_2)s^2 + (L_2 + k_2L_1 + k_1)s)}. \tag{22}$$

Equation (22) is function of  $b_0$ , the observer gains  $L_i$  and the controller gains  $k_i$ . The bandwidth parameterization is used to reduce the calculation of the  $L_i$  to the selection of the parameter  $\omega_o$  named observer bandwidth. Likewise, the  $k_i$  values are made dependent on the parameter  $\omega_c$  known as controller bandwidth.

Consider the state space representation of the extended model (5)

$$\begin{aligned} \begin{bmatrix} \dot{x}_1 \\ \dot{x}_2 \\ \dot{x}_3 \end{bmatrix} &= \underbrace{\begin{bmatrix} 0 & 1 & 0 \\ 0 & 0 & 1 \\ 0 & 0 & 0 \end{bmatrix}}_A \begin{bmatrix} x_1 \\ x_2 \\ x_3 \end{bmatrix} + \underbrace{\begin{bmatrix} 0 \\ b_0 \\ 0 \end{bmatrix}}_B u + \underbrace{\begin{bmatrix} 0 \\ 0 \\ 1 \end{bmatrix}}_E h \\ y &= \underbrace{\begin{bmatrix} 1 & 0 & 0 \end{bmatrix}}_C \begin{bmatrix} x_1 \\ x_2 \\ x_3 \end{bmatrix} \end{aligned} \tag{23}$$

whose matrix form is

$$\begin{aligned} \dot{x} &= Ax + Bu + Eh \\ y &= Cx, \end{aligned} \tag{24}$$

with  $x = [x_1 \ x_2 \ x_3]^T$ . Similarly, the matrix form of observer (6) is given by (25) with  $z = [z_1 \ z_2 \ z_3]^T$  and  $L = [L_1 \ L_2 \ L_3]^T$ .

$$\dot{z} = Az + Bu + L(Cx - Cz). \tag{25}$$

Let  $e = x - z$  be the estimation error. Its dynamic behavior is given by (26) and it is obtained after subtracting (25) from (24).

$$\dot{e} = (A - LC)e + Eh. \tag{26}$$

Assuming that  $h$ , even it is unknown, it is also differentiable and bounded, the observer gains can be calculated through pole placement. In [4], it is proposed that the three poles be located at position  $-\omega_o$  in the left semi-plane such as

$$sI - (A - LC) = (s + \omega_o)^3. \tag{27}$$

Thus, the parameterization of the observer gains (28) is obtained as a function of  $\omega_o$  by solving for both sides of (27) and comparing factors.

$$L_1 = 3\omega_o \quad L_2 = 3\omega_o^2 \quad L_3 = \omega_o^3. \tag{28}$$

On the other hand, the controller gains design takes into account the frequency representation of the modified plant (8) and the control action (9) to obtain the closed loop transfer function

$$G_Y(s) = \frac{k_1}{s^2 + k_2s + k_1}. \tag{29}$$

According to the characteristic equation of (29), the closed loop poles depends on selection of the gains  $k_1$  and  $k_2$ . Then, following the approach from [4], the poles are located at  $-\omega_c$  as in (30) and the controller gains parameterization of (31) is derived.

$$s^2 + k_2s + k_1 = (s + \omega_c)^2 \tag{30}$$

$$k_1 = \omega_c^2 \quad k_2 = 2\omega_c. \tag{31}$$

The bandwidth parameterization from (28) and (31) is used in (22) to obtain

$$G_A(s) = \frac{(3\omega_c^2\omega_o + 6\omega_c\omega_o^2 + \omega_o^3)s^2 + (2\omega_c\omega_o^3 + 3\omega_c^2\omega_o^2)s + \omega_c^2\omega_o^3}{b_0[s^3 + (3\omega_o + 2\omega_c)s^2 + (3\omega_o^2 + 6\omega_c\omega_o + \omega_c^2)s]}. \tag{32}$$

Therefore, by proper selection of  $b_0$ ,  $\omega_c$  and  $\omega_o$ , the second-order LADRC estimates and rejects the load disturbances acting on the loop.

Now, let the following FOPDT system be the plant to be controlled

$$G(s) = \frac{K}{Ts + 1} e^{-ls}, \tag{33}$$

where  $K$  is the static gain,  $T$  is the apparent time constant and  $l$  is the apparent delay or dead time [21].

If  $G_n(s)$  is considered as a nominal FOPDT plant, then, following the scaling and bandwidth parameterization theorem [see (21)], the model (33) can be treated as a scaled version of (34) in which  $k = K$ ,  $\omega_p = 1/T$  and  $\Theta = l/T$  as shown in (35).

$$G_n(s) = \frac{1}{s + 1} e^{-\Theta s} \tag{34}$$

$$G(s) = K \left( \frac{1}{\frac{s}{1/T} + 1} \right) e^{-\frac{1}{T} \frac{s}{1/T}}. \quad (35)$$

Hence, through some mathematical manipulation, the scaled controller  $\bar{G}_A(s) = (1/k)G_A(s/\omega_p)$  leads to the definition of the new set of LADRC parameters

$$\bar{b}_0 = \frac{Kb_0}{T^2} \quad \bar{\omega}_c = \frac{\omega_c}{T} \quad \bar{\omega}_o = \frac{\omega_o}{T}. \quad (36)$$

In conclusion, if a stable second-order LADRC with parameters  $b_0$ ,  $\omega_c$  and  $\omega_o$  is designed for the nominal system (34), then, the scaled LADRC with parameters  $\bar{b}_0$ ,  $\bar{\omega}_c$  and  $\bar{\omega}_o$  is suitable for the control of the general FOPDT plant (33).

### 3. Multiobjective Optimization Design Procedure

In this section, the generalities of the multiobjective optimization approach used to address the LADRC tuning problem are presented. Particularly, the steps of a Multiobjective Optimization Design (MOOD) procedure are briefly explained and the pertinence of this approach for the tuning problem is explored by means of a numerical example.

When designing a controller, the tuning process or solution obtained is strongly dependent on the desired performance for the closed loop. The behavior of the output, control action, and any other signals of interest is usually measured through some performance indices or design objectives. If these indices are wanted to be minimized or maximized, then, an optimization statement can be formulated.

For each minimized or maximized index, a particular solution is obtained. Therefore, if different design objectives are optimized simultaneously, then, multiple solutions can be suitable for the tuning of the same controller, not implying that one is better than the other, but suggesting that a solution can be selected with a particular trade-off among the aforementioned conflicting objectives. In this case, if the designer is interested, for example, in the simultaneous minimization of two performance indices, a MOOD procedure could aid in the tuning problem.

A MOOD procedure comprises three fundamental steps [22].

1. Multiobjective Problem (MOP) definition: The design objectives of interest are stated as well as the decision variables and the possible constraints.
2. Optimization Process (OP): An algorithm is selected to search throughout the decision space for the approximations of the optimal solutions (Pareto Set) and their corresponding objective values (Pareto Front). This algorithm should fulfill some desirable characteristics in order to provide the designer with useful solutions.
3. Multicriteria Decision Making (MCDM): Specialized visualization techniques are employed to analyze the Pareto Front and Pareto Set approximations. The best solution is the one that meets the designer's preferences.

As an example, Figure 3 illustrates the concepts of Pareto dominance, Pareto Front and Pareto Set for the biobjective optimization problem  $\min_{\theta} J(\theta) = [J_1(\theta), J_2(\theta)]$  with decision variables  $\theta = [\theta_1, \theta_2]$ . The decision vectors  $\theta^1, \dots, \theta^5$  dominates the vectors  $\theta^6$  and  $\theta^7$  because the objective vectors  $J(\theta^1), \dots, J(\theta^5)$  are not worse than  $J(\theta^6), J(\theta^7)$  in both objectives and are better in at least one objective.

In order to explore the suitability of the multiobjective optimization approach for the LADRC tuning problem, the responses to an unitary step load disturbance ( $\tilde{r} = 0, d = 1$ ) and to an unitary step setpoint ( $\tilde{r} = 1, d = 0$ ) of the closed loop of Figure 2 with  $G(s)$  as (37) were obtained for different combinations of the three LADRC tuning parameters in the search space:  $b_0 \in [5, 35]$ ,  $\omega_c \in [1, 25]$  rad/s,  $\omega_o \in [1, 25]$  rad/s, and following a grid method with  $\Delta b_0 = 1$  and  $\Delta \omega_o = \Delta \omega_c = 0.2$  rad/s.

$$G_e(s) = \frac{1}{s+1} e^{-s}. \quad (37)$$

Initially, the LADRC stability region was analyzed. Figure 4 shows the pairs  $(\omega_c, \omega_o)$  for the critical gain nominal values  $b_0 = 5, 15, 35$  that produce a stable output in system (37). From this figure, it is noted that as the nominal value of the critical gain increases, more pairs  $(\omega_c, \omega_o)$  appears in the stability region which represent more possible combinations for the LADRC tuning. In other words, there exists a stability bound that moves in the  $(\omega_c, \omega_o)$  increasing direction as a higher value of  $b_0$  is selected.

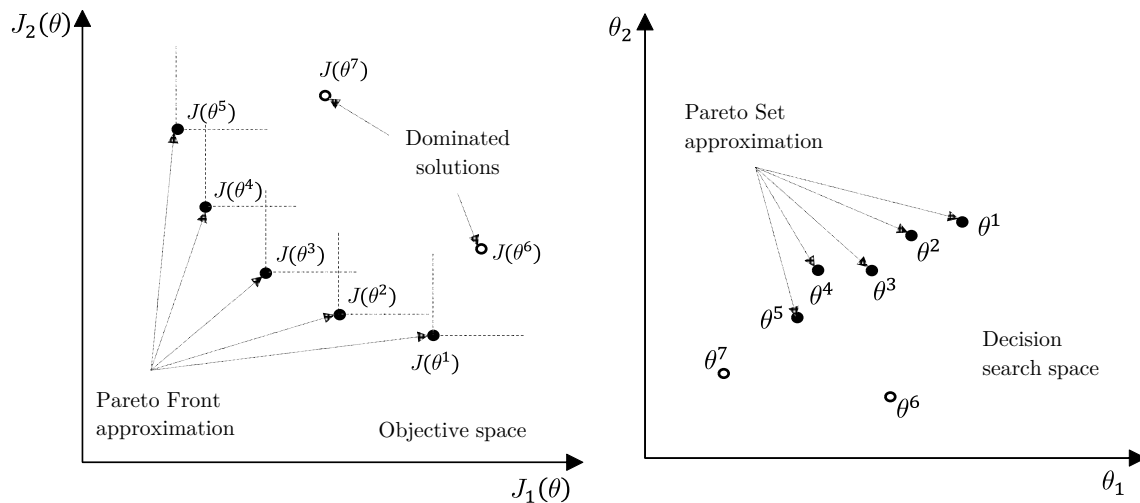


**Figure 3.** Pareto dominance, Pareto Front and Pareto set in a bidimensional case. There are no solution vectors dominating  $\theta^1, \dots, \theta^5$  so these solutions are the approximation of the Pareto Set and their corresponding objective vectors  $J(\theta^1), \dots, J(\theta^5)$  are the approximation of the Pareto Front.

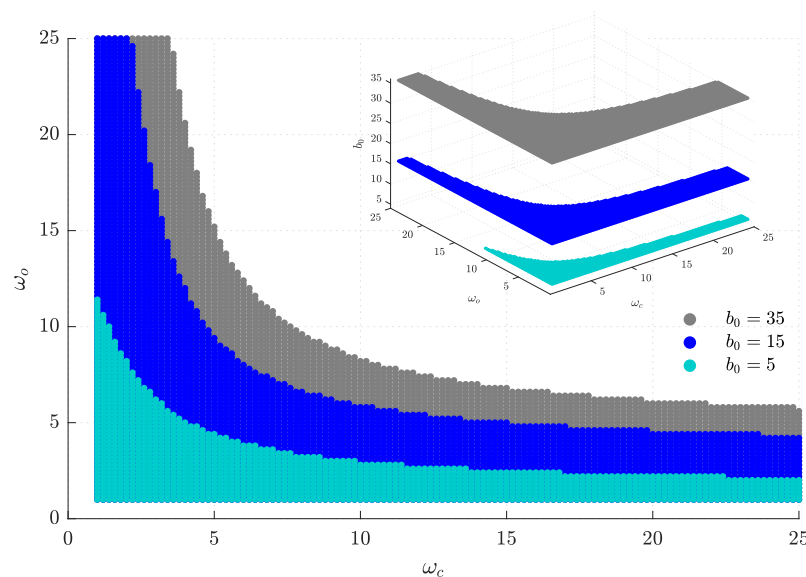


**Figure 4.** Closed loop stability regions for  $G_e(s)$ . Each point in the region represents a combination of parameters producing a stable output. For each value of  $b_0 \in [5, 35]$  there exist pairs  $(\omega_c, \omega_o)$  that produce a stable output. The  $b_0 = 5, 15, 35$  values are plotted as examples to illustrate the shape and behavior of the stability region.

Once the LADRC stability region was obtained, interest was put in the performance computed with those combinations of parameters. Particularly, the ITSE for load disturbance rejection, the robustness, and the Total Variation of control action (TV) were defined as design objectives as stated in Table 1.

**Table 1.** Design objectives for the performance evaluation of the Linear ADRC (LADRC).

Index/Design Objective	Definition
Integral of the time weighted squared error value	$ITSE = \int_{t=0}^{t_{98\%}} t \cdot (r(t) - y(t))^2 dt$
Total variation of the control action	$TV = \sum_{i=1}^{t_{98\%}}  u_{i+1} - u_i $
Mixed robustness	$\epsilon = \sup_{\omega} ( S(j\omega)  +  T(j\omega) ).$

Closed loop robustness is usually measured through the maximum peak of the sensitivity function  $M_S$  and the maximum peak of the complementary sensitivity function  $M_T$  such as  $1.3 < M_S < 2$  and  $M_T < 1.25$  [23]. In this work, a robustness measure denoted by  $\epsilon$  is adopted which is defined in [24] as the structured singular value of matrix  $M$  from a  $M - \Delta$  configuration with a diagonal block structure.

The  $\epsilon$  index has been previously used in [14] to quantify the robust stability of the closed loop system with the LADRC and is computed as the maximum peak of the sum of the magnitudes of the frequency responses of the sensitivity function  $S(j\omega)$  and the complementary sensitivity function  $T(j\omega)$ . The lower the value of  $\epsilon$ , the more robust the closed loop system.

A first look at the minimum ITSE value inside the stability region shows that  $ITSE_{\min 1} = 0.82$  for the solution  $b_{01} = 17, \omega_{c1} = 1.8 \text{ rad/s}, \omega_{o1} = 23.6 \text{ rad/s}$ . However, the associated robustness of  $\epsilon_1 = 5.93$  is regarded as poor. If the constraint  $\epsilon \leq 3$  is imposed on the robustness index, then a new solution  $b_{02} = 24, \omega_{c2} = 2 \text{ rad/s}, \omega_{o2} = 21 \text{ rad/s}$  is found with an  $ITSE_{\min 2} = 1.13$  and a corresponding robustness of  $\epsilon_2 = 2.99$ .

On the other hand, a search for the most robust controller results in the parameters  $b_{03} = 15, \omega_{c3} = 19.8 \text{ rad/s}, \omega_{o3} = 1 \text{ rad/s}$  which produce  $\epsilon_{\min 3} = 1.38$  but with an extremely high ITSE value of  $ITSE_3 = 113.51$ . Also, if the ITSE is constrained such as  $ITSE \leq 2$ , then the new solution is  $b_{04} = 19, \omega_{c4} = 21 \text{ rad/s}, \omega_{o4} = 2.8 \text{ rad/s}$  with a robustness  $\epsilon_{\min 4} = 2.02$  and a time performance index  $ITSE_4 = 1.99$ .

Table 2 comprises the solutions and performance comparison discussed above. Some additional indices as  $M_S, M_T$ , total variation of control action for disturbance rejection ( $TV_d$ ), and total variation of control action for setpoint following ( $TV_s$ ) are included as complementary information. Note that each of the LADRC set of parameters can be considered as optimal only respect to the corresponding minimized index. For example, the solution  $(b_{02}, \omega_{c2}, \omega_{o2})$  is optimal respect to the ITSE, but the robustness obtained is the maximum allowed according to the constraint.

**Table 2.** Comparison of LADRC performance in control of  $G_e(s)$ .

Desired Performance	LADRC Parameters	$M_S$	$M_T$	$\epsilon$	ITSE	$TV_d$	$TV_s$
min ITSE	$b_{01} = 17$ $\omega_{c1} = 1.8 \text{ rad/s}$ $\omega_{o1} = 23.6 \text{ rad/s}$	3.45	2.48	5.93	0.82	3.14	2.50
min ITSE $\epsilon \leq 3$	$b_{02} = 24$ $\omega_{c2} = 2 \text{ rad/s}$ $\omega_{o2} = 21 \text{ rad/s}$	1.98	1.16	2.99	1.13	1.40	1.32
min $\epsilon$	$b_{03} = 15$ $\omega_{c3} = 19.8 \text{ rad/s}$ $\omega_{o3} = 1 \text{ rad/s}$	1.19	1.00	1.38	113.51	1.02	33.87
min $\epsilon$ $ITSE \leq 2$	$b_{04} = 19$ $\omega_{c4} = 21 \text{ rad/s}$ $\omega_{o4} = 2.8 \text{ rad/s}$	1.50	1.01	2.02	1.99	1.10	29.25

In addition to the solutions reported in Table 2, there are other sets of LADRC parameters within the stability region that offer a compromise between disturbance rejection, quantified by ITSE, and robustness. To search for these alternatives, the Pareto dominance definition was applied over the total of parameters combinations, restricting the robustness measure to the range  $\varepsilon \in [2, 3]$  which represents a maximum sensitivity in the range  $M_S \in [1.3, 2]$  and a maximum complementary sensitivity in the interval  $M_T \in [1, 1.4]$ .

Figure 5a shows the Pareto Front approximation for the simultaneous minimization of ITSE for disturbance rejection and robustness. As expected, the ITSE can not be improved (decreased) without weakening the robustness. Likewise, a more robust closed loop system is possible as long as the ITSE value is allowed to increase. The solutions  $(b_{02}, \omega_{c2}, \omega_{o2})$  and  $(b_{04}, \omega_{c4}, \omega_{o4})$  from Table 2 would be located around the upper and bottom ends of the Pareto Front approximation, respectively.

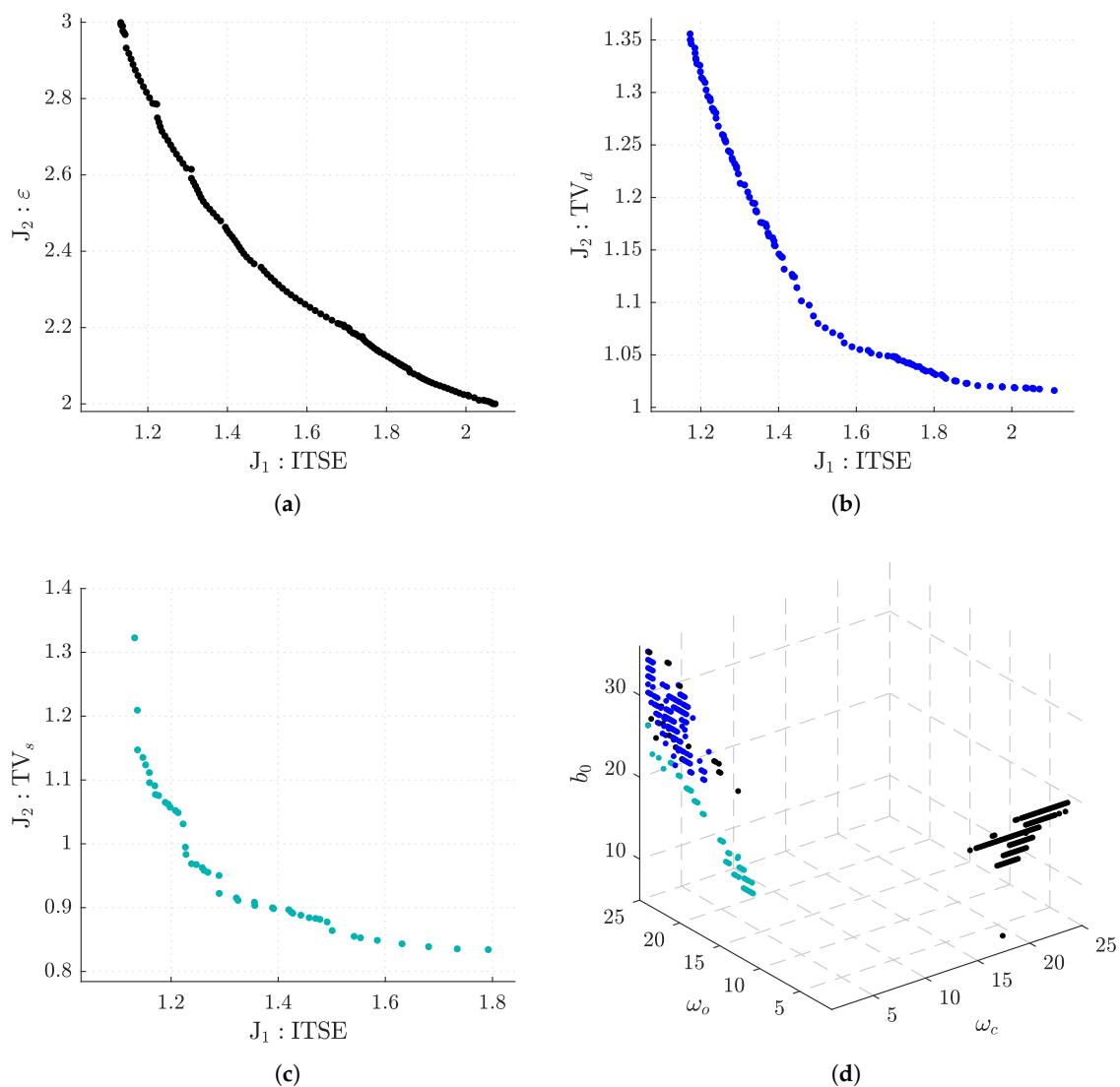


**Figure 5.** Pareto Fronts and Pareto Sets approximations for minimization of two design objectives  $J_1$  and  $J_2$ . (a) the Pareto Front approximation for the simultaneous minimization of ITSE for disturbance rejection and robustness. (b) the Pareto Front approximation for minimization of ITSE and TV for disturbance rejection ( $TV_d$ ). (c) the approximation of the Pareto Front when the ITSE for disturbance rejection is minimized simultaneously with the TV of the unitary setpoint ( $TV_s$ ). (d) the Pareto Sets approximations for the three said cases.

From other point of view, Figure 5b is the Pareto Front approximation for minimization of ITSE and TV for disturbance rejection ( $TV_d$ ) and Figure 5c is the approximation of the

Pareto Front when the ITSE for disturbance rejection is minimized simultaneously with the TV of the unitary setpoint ( $TV_s$ ). These figures show that there is also a compromise between the ITSE performance and the control efforts.

Finally, the Pareto Sets approximations for the three said cases are presented in Figure 5d. Note that the optimal values for the nominal critical gain are higher than  $b_0 = 1$ , which would be the nominal value ( $b_0 = K/T$ ) computed from the model (37), as is commonly suggested in literature. Moreover, in the solutions with a compromise between ITSE and robustness, the controller bandwidth can be selected to be greater than the observer bandwidth ( $\omega_c > \omega_o$ ) or vice versa ( $\omega_c < \omega_o$ ). Nevertheless, for a compromise between ITSE and the total variation of the control action, a selection of parameters in which  $\omega_c < \omega_o$  seems more appropriated.

The case study addressed in this section gave some insight into the LADRC performance in the control of a FOPDT system. In summary, there exist a trade-off between the disturbance rejection performance of the LADRC and its robustness. The LADRC parameters that produce this compromise are Pareto optimal and can be searched through an optimization process where the objectives related to disturbance rejection and robustness are minimized simultaneously. Besides, the definition of constraints over the objective and search spaces could drive the optimization process to solutions that meet some desired additional performance. If the aforementioned optimization procedure is applied over a group of plants of the same kind, then the Pareto optimal alternatives could be used to derive tuning rules reflecting the desired trade-off.

#### 4. LADRC Tuning by Multiobjective Optimization

For the tuning problem of the second-order LADRC related to the control of FOPDT systems, a MOOD procedure was applied to a group of nominal plants in the form of (34) which was obtained by varying the nominal delay from  $\Theta = 0.5$  to  $\Theta = 5$  with a change of  $\Delta\Theta = 0.1$ .

The FOPDT systems can be characterized based on the normalized dead time  $\tau = l/(l + T)$  with  $0 \leq \tau \leq 1$  [25]. Particularly, a system is lag-dominated if  $\tau$  is small, balanced if  $\tau$  is around 0.5 and delay-dominated if  $\tau$  is large [26]. In terms of the nominal delay,  $\tau$  can be written as

$$\tau = \frac{\Theta}{\Theta + 1}. \quad (38)$$

Thus, the MOOD procedure was applied to plants with  $\tau$  ranging from 0.09 to 0.83, which includes lag-dominated, balance, and delay-dominated processes. The MOOD results were used to fit the optimal solutions for the LADRC parameters and the fitting curves were scaled to obtain the tuning rules as functions of the known FOPDT parameters. In this section, each step of the MOOD procedure and the data processing of solutions are explained in depth.

##### 4.1. MultiObjective Problem Definition

The first stage of the MOOD procedure implies the definition of the decision space, the objective space, and the possible constraints. The decision variables are selected from the parametric controller; the objective space is related to the desired performance, and finally, constraints are the design limitations imposed on the overall concept.

The plant to be controlled corresponds to the FOPDT nominal model (34). Note that any controller designed for this plant can be scaled afterwards according to (36).

The following scaling for observer bandwidth were also adopted:

$$\omega_o = k_o \omega_c, \quad k_o > 1, \quad (39)$$

which indicates that LADRC parameters meeting the relation  $\omega_c < \omega_o$  are preferred. This additional scaling is commonly suggested in literature (e.g., in [4,11,12]).

The transfer function (40) is obtained by substituting (39) in (32).

$$G_A(s) = \frac{(3k_o\omega_c^3 + 6k_o^2\omega_c^3 + k_o^3\omega_c^3)s^2 + (2k_o^3\omega_c^4 + 3k_o^2\omega_c^4)s + k_o^3\omega_c^5}{b_0[s^3 + (3k_o\omega_c + 2\omega_c)s^2 + (3k_o^2\omega_c^2 + 6k_o\omega_c^2 + \omega_c^2)s]}. \quad (40)$$

Choosing a value of  $k_o = 10$ , the corresponding controller to tune is

$$G_A(s) = \frac{1630\omega_c^3s^2 + 2300\omega_c^4s + 1000\omega_c^5}{b_0(s^3 + 32s^2 + 361\omega_c^2s)}, \quad (41)$$

with the decision variables:

$$\theta = [b_0, \omega_c]. \quad (42)$$

Two design objectives were selected: the ITSE for the response to a unitary step load disturbance and the mixed robustness index  $\varepsilon$ . Thus, the complete multiobjective problem is stated as

$$\min_{\theta} J(\theta) = [J_1(\theta), J_2(\theta)] \quad (43)$$

$$J_1(\theta) = \text{ITSE}(\theta) \quad (44)$$

$$J_2(\theta) = \varepsilon(\theta) \quad (45)$$

$$\theta = [b_0, \omega_c], \quad (46)$$

subject to

Stable in closed loop

$$\begin{aligned} J_1(\theta) &\leq \text{ITSE}_{\text{SIMC}} \\ 2 &\leq J_2(\theta) \leq 3 \\ 1 &\leq b_0 \leq 200 \\ 0.1 &\leq \omega_c \leq 20 \end{aligned} \quad (47)$$

The constraints on design objectives were selected taking into account the performances offered over the group of nominal plants by classical PID tuning rules as IMC [27], SIMC [28], and AMIGO [29], and the LADRC tuning method from [14]. The upper limit of  $J_1(\theta)$  was set as the ITSE value obtained with the SIMC approach such that the desired closed loop time constant was equal to the apparent delay  $l$ . The SIMC tuning produced the highest ITSE for each plant compared to the LADRC from [14] and the other PID controllers.

Similarly, the lower limit of  $J_2(\theta)$  is the approximation of the robustness obtained with the AMIGO tuning rules, and its upper limit is approximately the robustness computed with the IMC method. The other controllers offer a robustness measure between these limits for all plants. What is more, the  $\varepsilon(\theta)$  limits are related to the commonly adopted limits for maximum sensitivity and maximum complementary sensitivity.

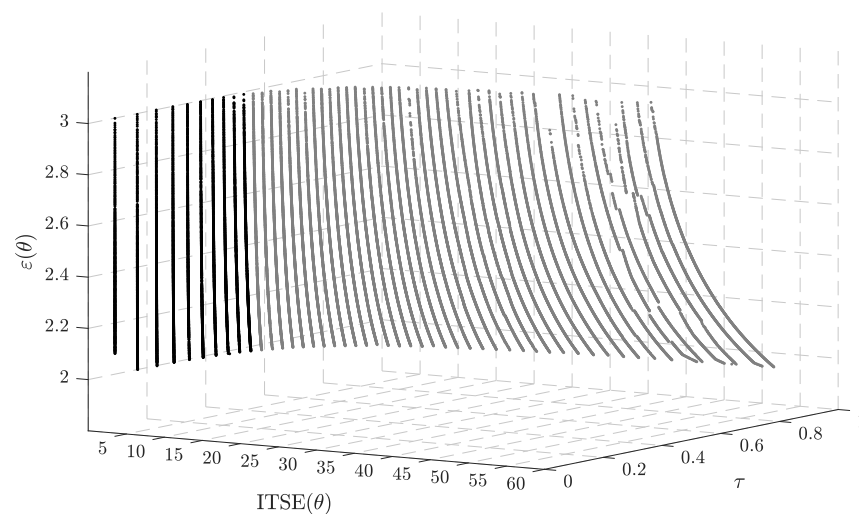
The search space for decision variables was specified following the results from Section 3 where it was shown that to increase  $b_0$  contributes to a bigger stability region in terms of the bandwidths and, as a consequence, lower performance indices can be computed.

#### 4.2. Optimization Process

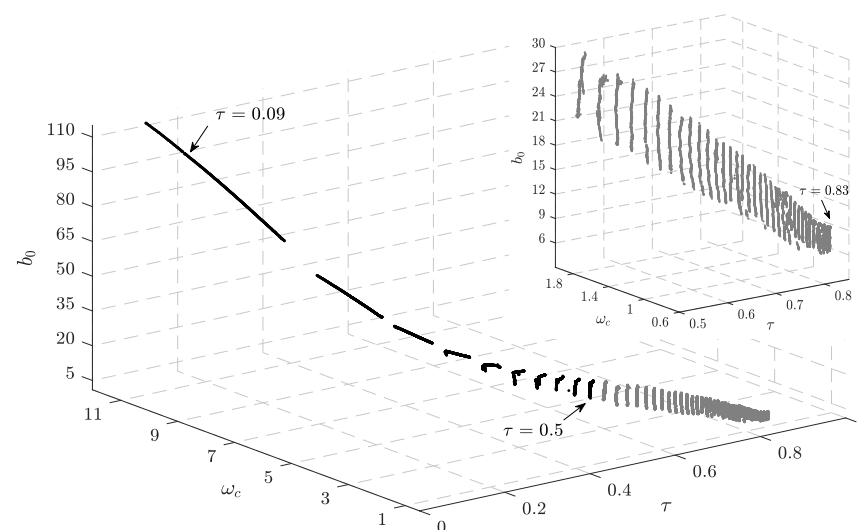
The evolutionary multiobjective algorithm  $\varepsilon^{\lambda}$ -MOGA [30] was used to perform the optimization process. This algorithm uses the epsilon-dominance concept to obtain Pareto Front and Pareto Set approximations with limited memory resources and preserving the diversity of the Front by adjusting its limits dynamically [31]. The algorithm parameters

were set to 200 individuals for main population, 8 individuals for auxiliary population, 1000 generations and 1000 divisions per dimension.

The Pareto Fronts and Pareto Sets approximations obtained for the complete group of nominal plants are presented in Figure 6. From Figure 6b, an interesting behavior is observed. The range of the decision variables for plants with  $\tau \leq 0.5$  is wider than for plants with  $\tau > 0.5$ . For instance, a robustness measure between 2 and 3 can be obtained for the plant with  $\tau = 0.09$  if the LADRC parameters are selected in the ranges  $b_0 \in [86, 115]$ ,  $\omega_c \in [11.6, 6.6]$ , whereas the same variation in robustness for plant with  $\tau = 0.833$  is achieved with  $b_0 \in [6.2, 9.2]$ ,  $\omega_c = [0.73, 0.71]$ . Another important feature is the decreasing trend in the decision variables as the normalized delay increases. However, the rate of change in both parameters tends to be greater for plants with  $\tau \leq 0.5$  than for plants with  $\tau > 0.5$ .



(a) Pareto Fronts approximations



(b) Pareto Sets approximations

**Figure 6.** Results from the optimization process for the complete group of nominal plants. Pareto Sets approximations for plants with  $\tau \leq 0.5$  (black) show that the LADRC parameters for this group have a wider range of variation and the rate of change in both parameters is greater compared to plants with  $\tau > 0.5$  (gray). An inset showing the Pareto Sets approximations for plants with  $\tau > 0.5$  is included for better visualization.

### 4.3. Multicriteria Decision Making

Once the Pareto Fronts and Pareto Sets approximations have been obtained, the last step in the MOOD procedure is the selection of the solution or candidate solutions preferred by the designer. Even if most of the preferences were taken into account in the optimization process, a final selection is needed. Depending on the number of design objectives, the visualization and graphical interpretation of the Pareto Front approximation is crucial. Some novel ideas to rank the potential solutions obtained by evolutionary algorithms in application to engineering problems are exposed in [32]. Likewise, an approach to the knee solution of the Pareto Front approximation for optimization problems with many objectives is addressed in [33].

According to the results from the optimization process, the following aspects were considered for the decision making stage.

- For data processing, two main groups were defined: *Group 1* containing data related to plants with a normalized delay  $\tau \leq 0.5$  and *Group 2* with data belonging to plants with  $\tau > 0.5$ .
- From each Pareto Front approximation, three design alternatives distributed along the front were selected.
- For *Group 1*, the selection was made using the entire Pareto Front approximation.
- For *Group 2*, the selection was made limiting the upper end of the front such that the highest value for  $\varepsilon(\theta)$  is 2.5. This criterion is based on the fact that the difficulty in controlling a process increases as its normalized delay increases [25]. Thus, for this group of plants, lower values of  $\varepsilon(\theta)$  are preferred which correspond to more robust closed loop systems.
- Selected solutions are compared in the objective space with other alternatives related to PID and LADRC tuning rules.

Consider the first group of nominal plants (*Group 1*). In order to select the three desired design alternatives, let the Pareto Fronts to be divided in two regions according to bounds imposed on the mixed robustness measure. The upper region comprises solutions for which  $2.5 \leq \varepsilon(\theta) \leq 3$  and the lower region includes those with  $2 \leq \varepsilon(\theta) < 2.5$ .

On each region, a point corresponding to the Nash solution was calculated by solving the problem [34]:

$$\max_{(J_1(\theta), J_2(\theta))} \left( J_1(\theta^2) - J_2(\theta) \right) \left( J_2(\theta^1) - J_1(\theta) \right), \quad (48)$$

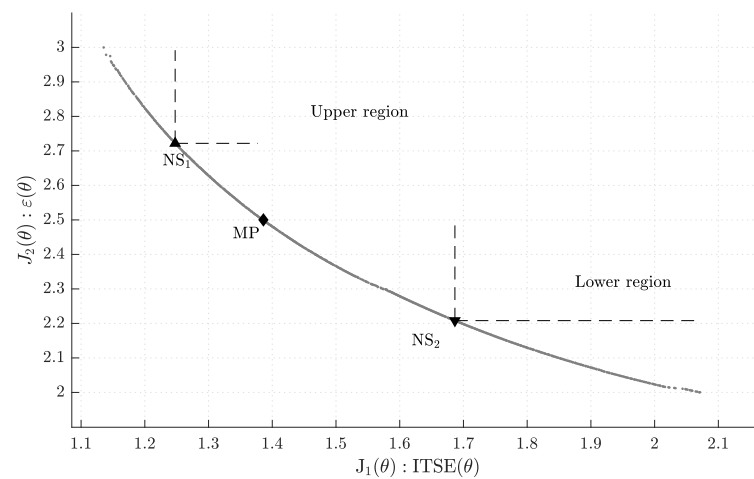
where  $J_1(\theta^2)$  is the optimal value (minimum) of the first design objective and  $J_2(\theta^1)$  is the point that minimizes the second cost function. The Nash solution  $(J_1(\theta), J_2(\theta))$  is considered a *fair* selection because it dominates the larger number of points in the rectangular area  $(J_1(\theta^2) - J_2(\theta)) (J_2(\theta^2) - J_1(\theta))$  [34].

The third solution for *Group 1* was selected as the midpoint of the Pareto Fronts. This is, the solution meeting the condition  $\varepsilon(\theta) = 2.5$ .

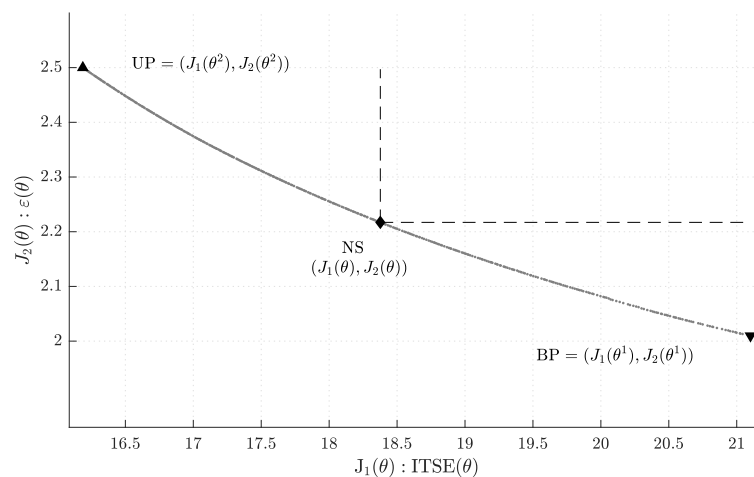
For the second group of plants (*Group 2*) the three selected solutions corresponds to the two ends of the front and the Nash solution.

Figure 7 illustrates the concepts explained and solutions selected taking as an example the Pareto Fronts approximations of the nominal plants with  $\tau = 0.5$  (*Group 1*) and  $\tau = 0.75$  (*Group 2*).

The complete set of Pareto Fronts approximations and selected solutions are presented in Figure 8. For comparison purposes, the performance obtained with the PID tuning methods IMC, SIMC, AMIGO, and the rules from [34] (SNS) are included for *group 1*. For *group 2*, the Pareto alternatives are compared with the SIMC and AMIGO approaches. Performance corresponding to the LADRC tuning rules from [14] (ADRC<sub>Z</sub>) are also shown for both groups. Note that the fronts move to the right in the objective space as the normalized delay increases. From this figure, the following remarks are derived.



(a)  $\tau = 0.5$



(b)  $\tau = 0.75$

**Figure 7.** Location of the selected solutions into the Pareto Fronts approximations taking as example two nominal plants. (a) For plants in *Group 1*, selected solutions are the Nash solution from upper region  $NS_1$ , the midpoint  $MP$ , and the Nash solution from lower region  $NS_2$ . (b) For plants in *Group 2* the selected solutions are the upper end  $UP$ , the Nash solution  $NS$ , and the bottom end  $BP$ .

- The performance obtained with the PID controllers tuned by the IMC, SIMC and SNS rules are in the dominance area of the Pareto Fronts belonging to plants from *Group 1*. Particularly, the SIMC points are dominated by the optimal solutions in all cases.
- For plants from *Group 2*, the performance obtained with the AMIGO tuning method is outside the Pareto Fronts approximations due to the constraint imposed on  $\epsilon(\theta)$ . However, the alternative solutions corresponding to the bottom end of the Fronts have better disturbance rejection with a reasonable level of robustness.
- The performance obtained with the  $ADRC_Z$  tuning rules is in the dominance area of the approximated Pareto Fronts for the entire set of nominal plants. Even though the  $ADRC_Z$  points are the results of fitting curves, they tend to move away from the Fronts as  $\tau$  increases which highlights their suboptimal feature.

With the MOOD procedure developed for the tuning problem of the second-order LADRC applied to FOPDT nominal systems, a set of Pareto optimal solutions with a trade-off between disturbance rejection and robustness was obtained. The distribution of these solutions in the decision search space can lead to different fitting curves depending on the preferred level of compromise between objectives. This idea is the core of the fitting procedure presented in the next section.

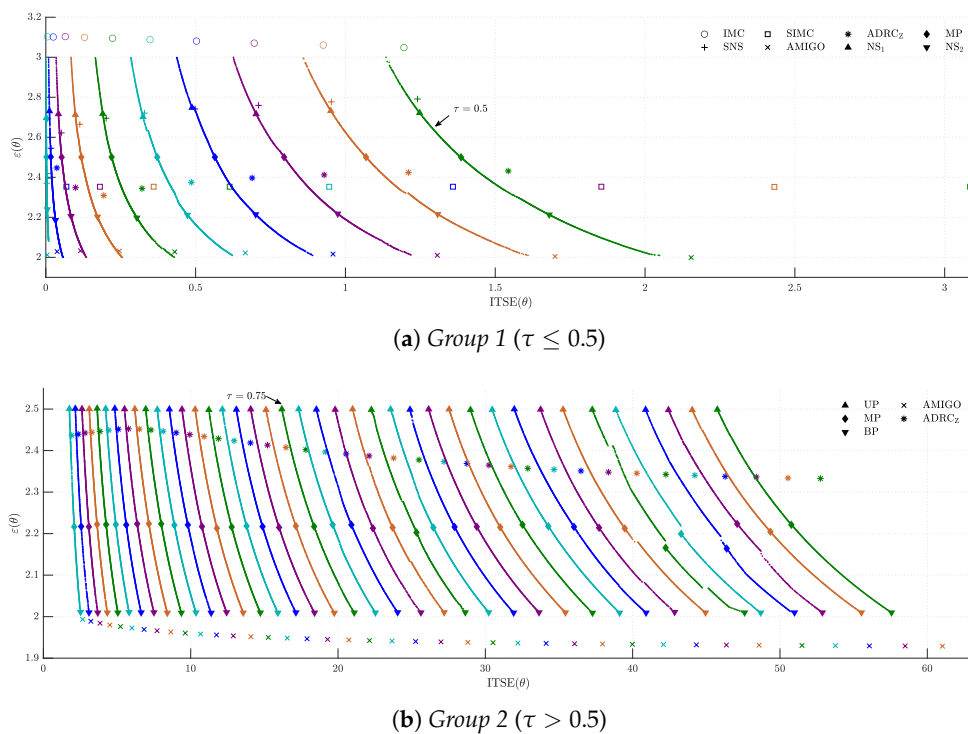


**Figure 8.** Pareto Fronts approximations and selected solutions for the complete set of nominal plants. Performance points obtained with the PID tuning methods IMC, SIMC, AMIGO, and SNS [34] as well as the LADRC tuning rules from [14] ( $ADRC_z$ ) are included for comparison. The SIMC points have been excluded from (b) for proper visualization because these alternatives are always dominated by the Pareto optimal solutions. Information related to the same plant has been plotted in the same color.

### 5. Tuning Rules for LADRC

The solutions obtained from the MOOD procedure correspond to the Pareto optimal LADRC parameters suitable to control FOPDT plants in the form of (34). These data were initially fitted to functions of the normalized delay  $\tau$ . Afterwards, the resulting expressions were scaled to obtain the LADRC tuning rules applicable to the control of the general FOPDT system (33).

Data were fitted separately for the two previously defined groups of plants. This was mainly because of the behavior observed in the rate of change of the parameters with respect to the variation in the normalized delay (see Figure 6b). Additionally, in each group, the three optimal solutions selected were used to fit three curves related to different levels of robustness taking  $\tau$  as independent variable. These levels of robustness were defined as follows.

- Low level ( $\epsilon_{low}$ ): The LADRC tuned by these approximation will offer a robustness around 2.7 for processes with  $\tau \leq 0.5$  and around 2.5 for plants with  $\tau > 0.5$ . For *Group 1*, the tuning rule was approximated using the Nash solutions of the upper regions of the Pareto Fronts ( $NS_1$ ). For *Group 2*, the curve was fitted using the upper ends of the fronts (UP).
- Medium level ( $\epsilon_{med}$ ): Processes with  $\tau \leq 0.5$  and controlled by LADRC tuned according to this formulae will have a robustness of approximately 2.5. In the case of plants with  $\tau > 0.5$ , the robustness of the closed loop will be around 2.3. The midpoints of the Pareto Fronts (MP) were used to approximate the tuning function in the first group of systems and the Nash solutions (NS) were used for the second group.
- High level ( $\epsilon_{high}$ ): The highest robustness of the closed loop will approximately 2.2 for systems with  $\tau \leq 0.5$  and 2.0 for plants meeting  $\tau > 0.5$ . In *Group 1* the approximation was done using the Nash solutions of the lower regions of the Pareto Fronts ( $NS_2$ ) and in *Group 2*, the bottom ends of the fronts (BP) were used instead.

The nominal values for the critical gain were fitted to power functions in the case of systems with  $\tau \leq 0.5$  and to polynomial functions for systems with  $\tau > 0.5$  such as

$$b_0 = \begin{cases} k_b \left( \frac{\tau}{1-\tau} \right)^{n_b}, & \tau \leq 0.5 \\ a_b \left( \frac{\tau}{1-\tau} \right)^2 + b_b \left( \frac{\tau}{1-\tau} \right) + c_b, & \tau > 0.5, \end{cases} \quad (49)$$

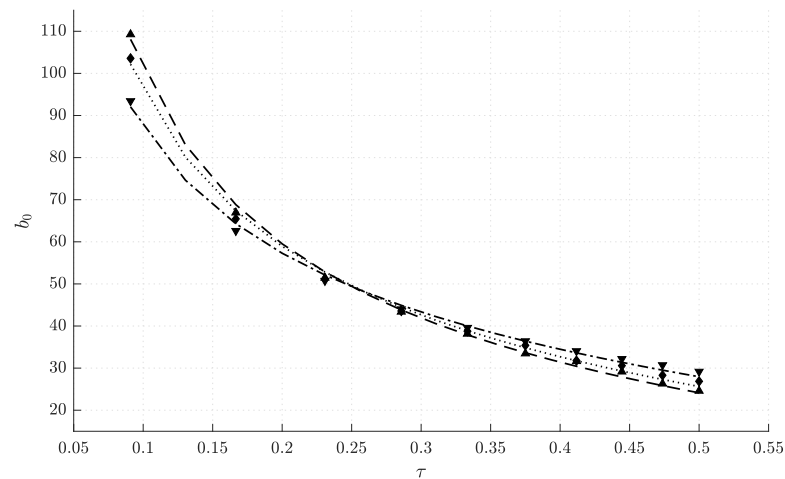
where  $k_b, n_b, a_b, b_b$  and  $c_b$  are constants.

On the other hand, the controller bandwidth values were fitted for both groups to power functions of the form

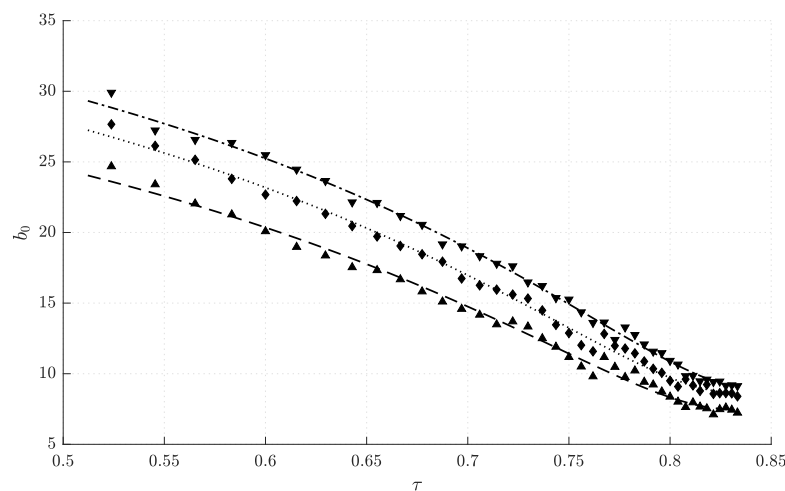
$$\omega_c = k_\omega \left( \frac{\tau}{1-\tau} \right)^{n_\omega}, \quad (50)$$

with  $k_\omega$  and  $n_\omega$  as constants.

The resultant fitting functions are presented in Figures 9 and 10, and the corresponding parameters for expressions (49) and (50) are reported in Table 3.

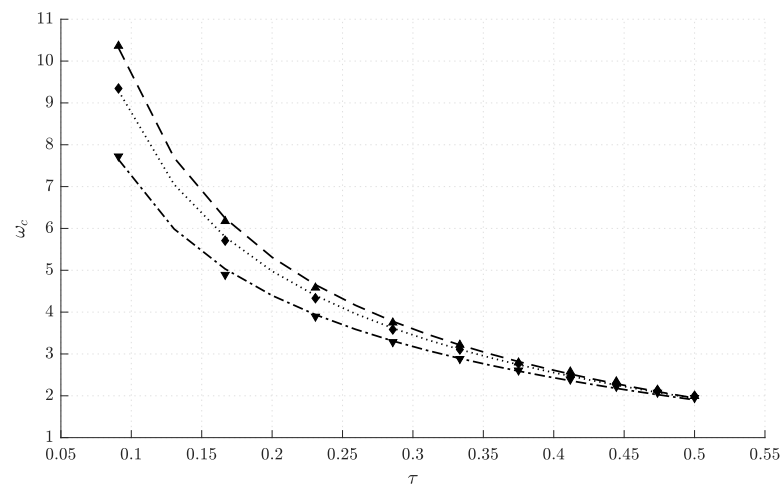


(a) Fitting for Group 1 ( $\tau \leq 0.5$ )

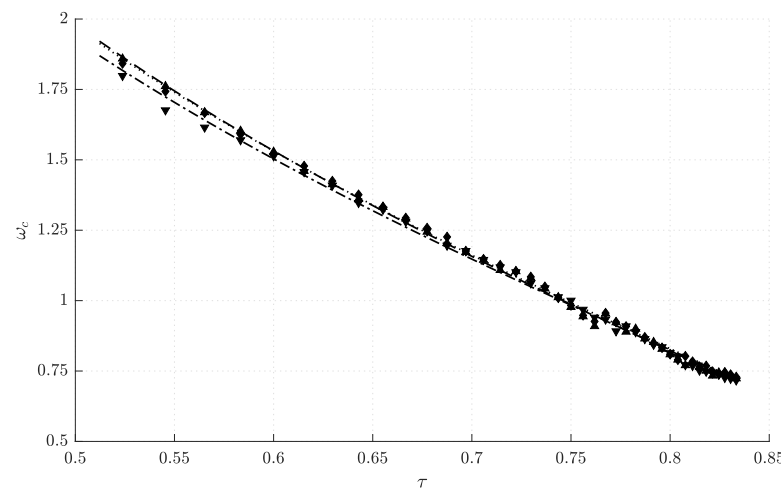


(b) Fitting for Group 2 ( $\tau > 0.5$ )

**Figure 9.** Tuning for nominal values of the LADRC critical gain. Markers indicate the optimal solutions NS<sub>1</sub> (▲), MP (◆), NS<sub>2</sub> (▼). Lines are the fitting functions for robustness levels  $\epsilon_{low}$  (—),  $\epsilon_{med}$  (⋯),  $\epsilon_{high}$  (---).



(a) Fitting for Group 1 ( $\tau \leq 0.5$ )



(b) Fitting for Group 2 ( $\tau > 0.5$ )

**Figure 10.** Tuning for LADRC controller bandwidth. Markers indicate the optimal solutions UP (▲), NS (◆), and BP (▼). Lines are the fitting functions for robustness levels  $\epsilon_{low}$  (---),  $\epsilon_{med}$  (···), and  $\epsilon_{high}$  (-·-).

As last step in the data processing, (49) and (50) were substituted in the corresponding scaled parameters of (36) to obtain the general LADRC tuning rules

$$\bar{b}_0 = \begin{cases} \frac{K}{T^2} \left[ k_b \left( \frac{\tau}{1-\tau} \right)^{n_b} \right], & \tau \leq 0.5 \\ \frac{K}{T^2} \left[ a_b \left( \frac{\tau}{1-\tau} \right)^2 + b_b \left( \frac{\tau}{1-\tau} \right) + c_b \right], & \tau > 0.5 \end{cases} \quad (51)$$

$$\bar{\omega}_c = \frac{1}{T} \left[ k_\omega \left( \frac{\tau}{1-\tau} \right)^{n_\omega} \right] \quad (52)$$

$$\bar{\omega}_o = \frac{10}{T} \left[ k_\omega \left( \frac{\tau}{1-\tau} \right)^{n_\omega} \right]. \quad (53)$$

Equations (51)–(53) are now dependent on the three FOPDT plant parameters which can be easily obtained for many processes by identification techniques.

As a summary, in Table 3 a guide for the tuning of the LADRC for the control of FOPDT plants is presented. Each of the defined levels of robustness represents a compromise between this objective and the disturbance rejection performance. This way, the designer is provided with three closed loop stable candidate controllers that could be tested on the system for the final decision.

**Table 3.** LADRC tuning guide.

1. Approximate the process dynamics with the First Order Plus Dead Time (FOPDT) model

$$G(s) = \frac{K}{Ts + 1} e^{-ls}.$$

2. Compute the normalized dead time. Note that the resulting normalized dead time meets the condition  $0 \leq \tau \leq 1$

$$\tau = \frac{l}{T + l}.$$

3. Decide whether the process belongs to Group 1:  $\tau \leq 0.5$  or Group 2:  $\tau > 0.5$  according to the normalized dead time computed in step 2. This classification indicates the level of robustness (quantified by  $\epsilon$ ) of each of the three candidate controllers.
4. Use the tables given below to select the appropriate coefficients for the tuning rules according to preferences on the robustness quality.

Group 1: $\tau \leq 0.5$				Group 2: $\tau > 0.5$			
Robustness level	$\epsilon_{\text{low}}$	$\epsilon_{\text{med}}$	$\epsilon_{\text{high}}$	Robustness level	$\epsilon_{\text{low}}$	$\epsilon_{\text{med}}$	$\epsilon_{\text{high}}$
Robustness, $\epsilon$	2.7	2.5	2.2	Robustness, $\epsilon$	2.5	2.3	2.0
$k_b$	24.129	25.632	27.952	$a_b$	1.145	1.238	1.121
$n_b$	-0.651	-0.601	-0.518	$b_b$	-11.110	-12.192	-11.921
$k_\omega$	1.946	1.938	1.903	$c_b$	34.443	38.682	40.601
$n_\omega$	-0.724	-0.681	-0.604	$k_\omega$	1.982	1.972	1.927
				$n_\omega$	-0.635	-0.625	-0.612

5. Substitute the coefficients selected in step 4, the static gain, and the apparent time constant in the following rules to compute the LADRC parameters

$$\bar{b}_0 = \begin{cases} \frac{K}{T^2} \left[ k_b \left( \frac{\tau}{1-\tau} \right)^{n_b} \right], & \tau \leq 0.5 \\ \frac{K}{T^2} \left[ a_b \left( \frac{\tau}{1-\tau} \right)^2 + b_b \left( \frac{\tau}{1-\tau} \right) + c_b \right], & \tau > 0.5 \end{cases} \quad \bar{\omega}_c = \frac{1}{T} \left[ k_\omega \left( \frac{\tau}{1-\tau} \right)^{n_\omega} \right] \quad \bar{\omega}_o = \frac{10}{T} \left[ k_\omega \left( \frac{\tau}{1-\tau} \right)^{n_\omega} \right].$$

6. Implement the second-order LADRC using the time domain or the frequency domain formulation.

Furthermore, the designer could vary the values of the LADRC parameters in the intervals obtained based on the proposed rules to adjust the performance according to the preferences. To help in this task, the tuning tool of Figure 11 has been developed in Matlab App Designer and is available at Matlab Central [18]. It requires as inputs the FOPDT model and through interaction with robustness level and manual tuning sliders, the user

can visualize the closed loop response and evaluate the second-order LADRC performance with the aid of some measures.

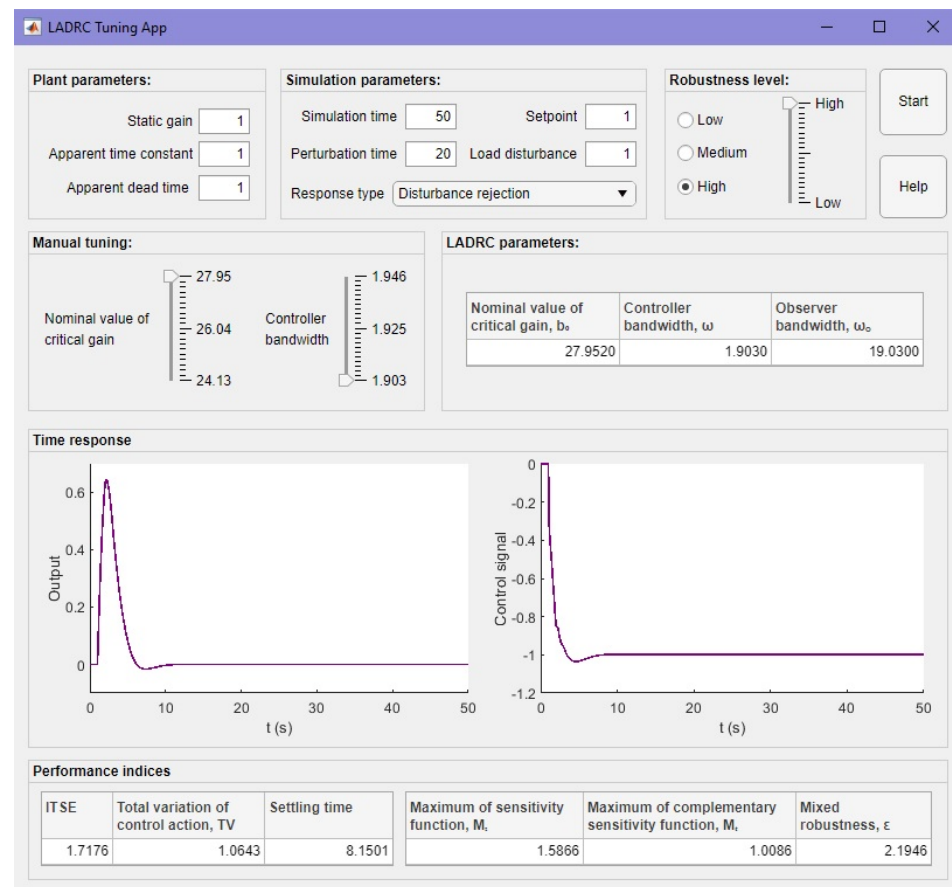


**Figure 11.** LADRC tuning tool. This Matlab App allows the automatic computation of the nominal value of the critical gain  $b_0$ , the controller bandwidth  $\omega_c$ , and the observer bandwidth  $\omega_o$  of the second-order LADRC for the control of a system approximated by a FOPDT model. Available at [18].

The tuning rules proposed in this section together with the developed tuning tool allow some degree of the designer involvement in the final selection of the LADRC parameters, but eliminates the time and complexity of performing the entire optimization process. The parameters computed by the proposed rules ensure closed loop stability as well as a reasonable compromise between disturbance rejection and loop robustness.

### 6. Validation of the LADRC Tuning Rules

In this section, two examples are presented to validate the proposed tuning rules. The load disturbance and setpoint responses are compared with the performance obtained from other controllers such as PID and LADRC tuned by different methods.

The performance indices in frequency domain  $M_S$ ,  $M_T$ ,  $\epsilon$  and in time domain ITSE, TV, and settling time ( $t_{98\%}$ , in seconds) were calculated.

#### 6.1. Example 1: A Lag-Dominated System

Consider the FOPDT lag-dominated system.

$$G_1(s) = \frac{1}{10s + 1} e^{-2s}. \tag{54}$$

The Tuning Guide is used to illustrate the parameters computation. Following the steps from Table 3:

1. From (54),  $K = 1$ ,  $T = 10$ , and  $l = 2$ .

2. The normalized dead time is

$$\tau = \frac{2}{10 + 2} = 0.17. \tag{55}$$

3. According to the normalized dead time from step 2, (54) belongs to Group 1 and thus, the three candidate controllers have robustness of approximately 2.7 ( $\epsilon_{low}$ ), 2.5 ( $\epsilon_{med}$ ), and 2.2 ( $\epsilon_{high}$ ).
4. For example, if a controller with a high robustness is preferred, the corresponding coefficients for the tuning rules are  $k_b = 27.952$ ,  $n_b = -0.518$  for computation of  $b_0$ ;  $k_\omega = 1.903$ ,  $n_\omega = -0.604$  for computation of  $\omega_c$  and  $\omega_o$ .
5. The nominal value of critical gain, the controller bandwidth, and the observer bandwidth are computed by substituting the coefficients from step 4 and the FOPDT parameters in the tuning rules. This is,

$$\bar{b}_0 = \frac{1}{100} \left[ 27.952 \left( \frac{0.17}{1 - 0.17} \right)^{-0.518} \right] = 0.643 \tag{56}$$

$$\bar{\omega}_c = \frac{1}{10} \left[ 1.093 \left( \frac{0.17}{1 - 0.17} \right)^{-0.604} \right] = 0.503 \tag{57}$$

$$\bar{\omega}_o = 1.903 \left( \frac{0.17}{1 - 0.17} \right)^{-0.604} = 5.031 \tag{58}$$

6. The parameters computed in step 5 can be used in the second-order LADRC for the control of plant (54).

Note that steps 4 and 5 from the above procedure must be repeated if a different robustness is desired. The LADRC parameters for the three levels of robustness ( $\epsilon_{low}$ ,  $\epsilon_{med}$ ,  $\epsilon_{high}$ ) are listed in Table 4. Parameters obtained with the tuning rules proposed in [14] (ADRC<sub>Z</sub>) are also listed together with those corresponding to the PID controllers tuned by the IMC, SNS (from [34]), SIMC and AMIGO methods. Figures 12 and 13 show the time responses.

**Table 4.** Parameters for the control of  $G_1(s)$ .

LADRC	$b_0$	$\omega_c$	$\omega_o$	PID	$K_p$	$T_i$	$T_d$
ADRC <sub>Z</sub>	0.349	1.950	0.960	IMC	4.320	10.800	0.751
$\epsilon_{low}$	0.688	0.624	6.243	SNS	3.420	5.475	0.970
$\epsilon_{med}$	0.674	0.580	5.795	SIMC	2.500	10.000	0
$\epsilon_{high}$	0.643	0.503	5.031	AMIGO	2.450	5.867	0.943

The resulting values for the performance indices are reported in Table 5. It can be seen that each of the proposed controllers offers a robustness level similar to one of the PID alternatives with a lower ITSE for disturbance rejection. Also, the output backs to steady state faster than with the IMC and SIMC.

Compared with the ADRC<sub>Z</sub> tuning rules, the three proposed controllers have a lower ITSE value and return the output to steady state faster in the case of a load disturbance. Note that with the  $\epsilon_{high}$  controller, a higher robustness level and better disturbance rejection performance can be achieved. Also, the total variation of the control action is lower for this alternative.

On the other hand, for setpoint following operation, a similar ITSE than ADRC<sub>Z</sub> is obtained with the  $\epsilon_{low}$  controller. However, it is worth noting that control actions produced by the three alternatives are smoother, which is reflected in the total variations indices calculated. This is mainly because the initial values of the control signals (sometimes

referred in literature as *proportional kick*) are significantly lower than those reached by the ADRC<sub>Z</sub> controller.

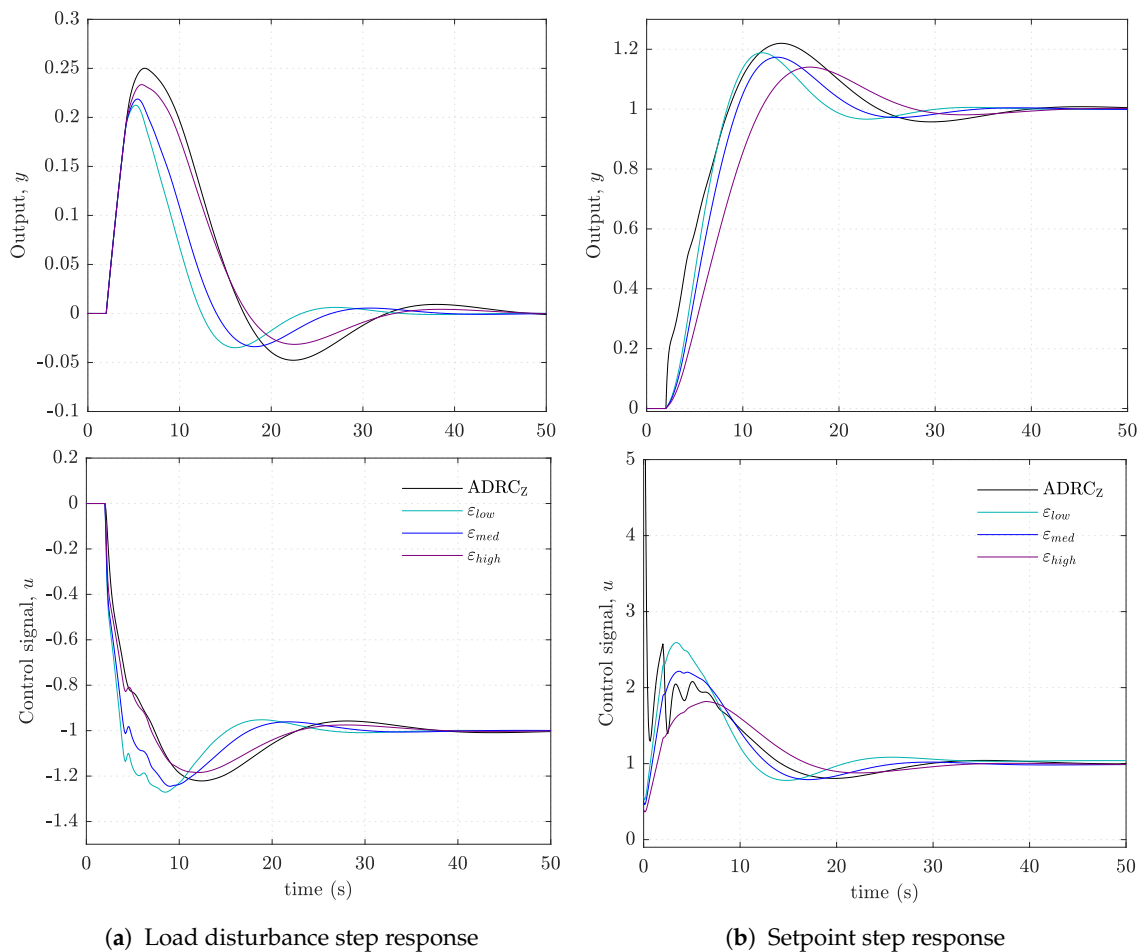


**Figure 12.** Closed loop time response of  $G_1(s)$  with the second-order LADRC tuned with the proposed rules. Comparison with the performance of ADRC<sub>Z</sub> controller.

**Table 5.** Performance comparison of proposed tuning rules with other tuning methods for control of  $G_1(s)$ . The  $\epsilon_{high}$  controller is more robust and offers a lower ITSE for disturbance rejection than the ADRC<sub>Z</sub> controller.

	$M_S$	$M_T$	$\epsilon$	Disturbance Rejection			Setpoint Following		
				ITSE	TV	$t_{98\%}$	ITSE	TV	$t_{98\%}$
IMC	2.032	1.097	3.103	2.485	1.358	44.1	2.788	60.985	8.7
SNS	1.767	1.181	2.545	1.738	1.331	26.7	4.023	48.914	18.5
SIMC	1.590	1.000	2.353	6.870	1.082	46.2	6.307	2.591	12.1
AMIGO	1.446	1.135	2.029	3.770	1.252	33.6	5.702	31.503	23.3
ADRC <sub>Z</sub>	1.583	1.345	2.447	3.688	1.537	43.3	12.488	14.699	35.4
$\epsilon_{low}$	1.842	1.489	2.771	1.227	1.743	29.9	12.672	4.298	26.4
$\epsilon_{med}$	1.735	1.392	2.544	1.652	1.636	33.1	14.685	3.520	29.1
$\epsilon_{high}$	1.598	1.258	2.236	2.982	1.438	31.4	19.404	2.562	25.9

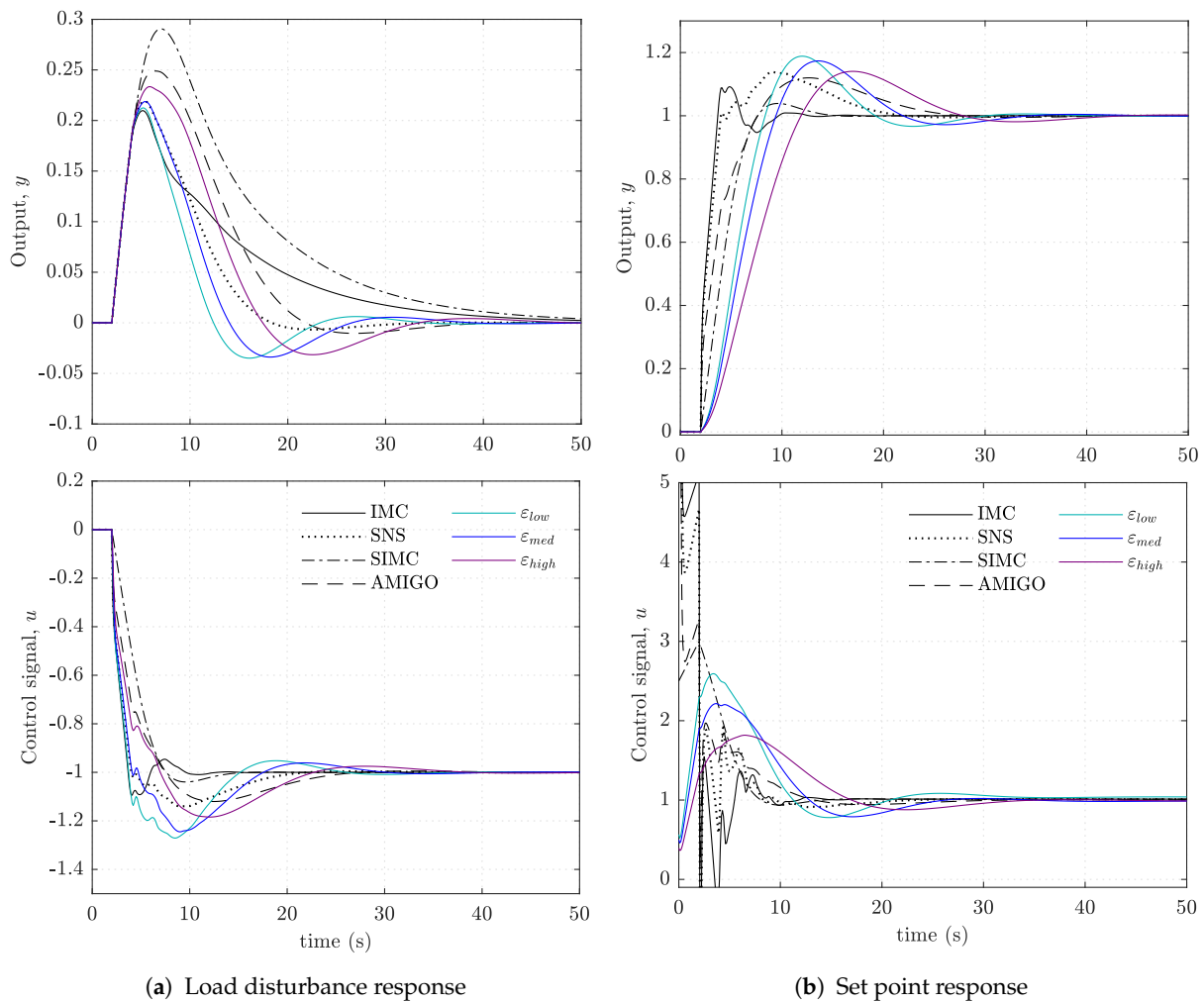


**Figure 13.** Closed loop time response of  $G_1(s)$  with the second-order LADRC tuned with the proposed rules. Comparison with the performance of PID controllers.

6.2. Example 2: A Delay-Dominated System

As second example, the following FOPDT delay-dominated system is analyzed:

$$G_2(s) = \frac{3}{0.25s + 1} e^{-s}. \tag{59}$$

The normalized delay for this plant is  $\tau = 0.80$ . The PID tuning rules IMC, SIMC and AMIGO, and the LADRC tuning rules from [14] ( $ADRC_z$ ) were used for comparison. In addition, the tuning rules for the second-order LADRC from [11] ( $ADRC_H$ ) were also taken into account. The latter are proposed for the control of high order plants, but can be used for self-regulatory FOPDT systems with nominal delay ( $\tau/T$ ) above 0.46 by approximating the plant into the form  $K/(Ts + 1)^n$  (Note that  $K$  and  $T$  have a different meaning than in (33)).

Figures 14 and 15 show the closed loop time response of  $G_2(s)$  with the LADRC and the PID controllers, respectively. The computed parameters are listed in Table 6 and performance indices are reported in Table 7.

**Table 6.** Parameters for the control of  $G_2(s)$ .

LADRC	$b_0$	$\omega_c$	$\omega_o$	PID	$K_p$	$T_i$	$T_d$
ADRC <sub>Z</sub>	359.316	5.029	16.140	IMC	0.173	0.650	0.195
ADRC <sub>H</sub>	345.819	2.521	33.007	SIMC	0.042	0.250	0
$\epsilon_{low}$	399.747	3.288	32.876	AMIGO	0.104	0.585	0.227
$\epsilon_{med}$	466.508	3.317	33.172				
$\epsilon_{high}$	521.205	3.301	33.007				

According to the indices obtained for disturbance rejection, the proposed controllers can improve the performance in at least one of the design objectives when compared to the PIDs. For example, The  $\epsilon_{med}$  controller is more robust and produces a lower ITSE than the PID tuned by the SIMC method. The same controller offers an improvement in robustness and disturbance rejection in comparison with ADRC<sub>Z</sub>.

On the other hand, the ITSE calculated from the load disturbance response with the three proposed controllers are lower than the ITSE obtained with the ADRC<sub>H</sub> controller. The corresponding total variations of control signals are also lower and the system output stabilizes faster, even in the case of a setpoint change. It should be noted that LADRC parameters for ADRC<sub>H</sub> were obtained setting an required additional tuning parameter  $k$  as 3.25 after some trial and error tests to guarantee the stability.

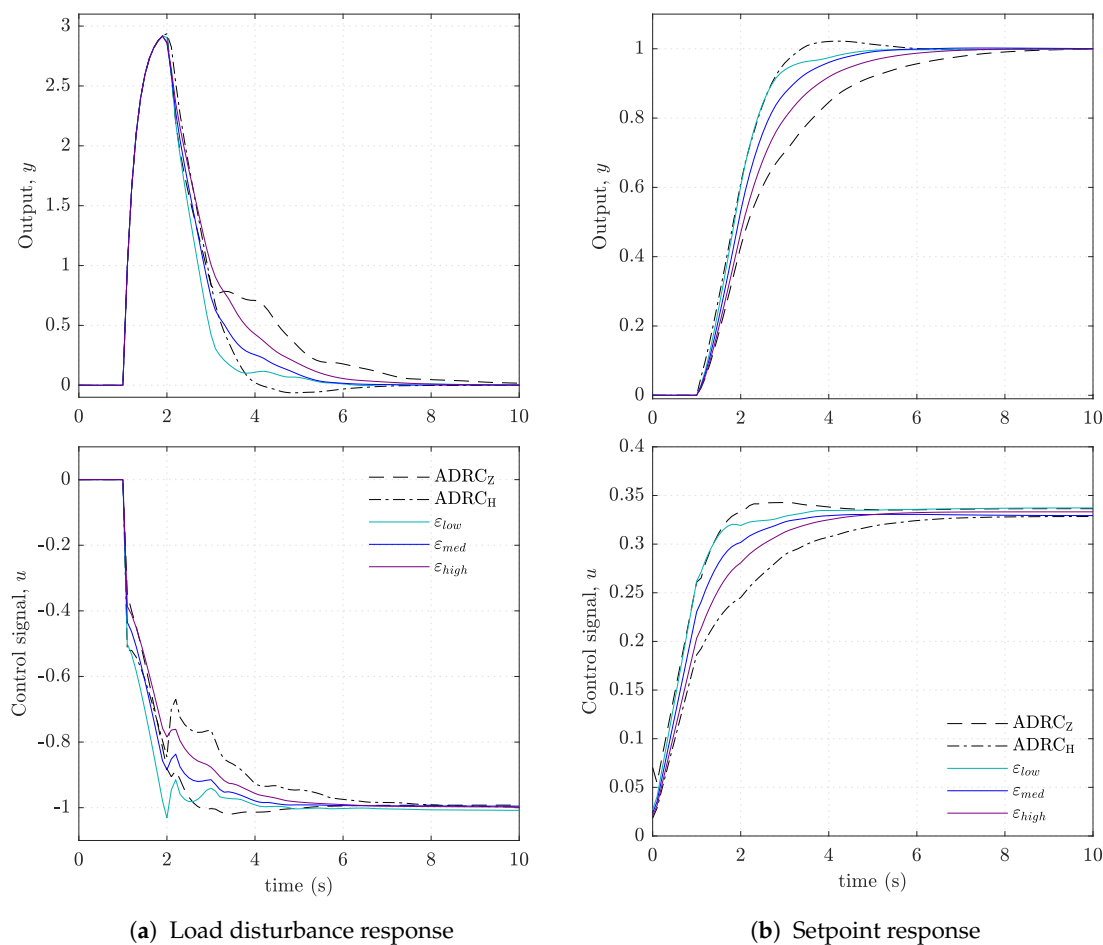
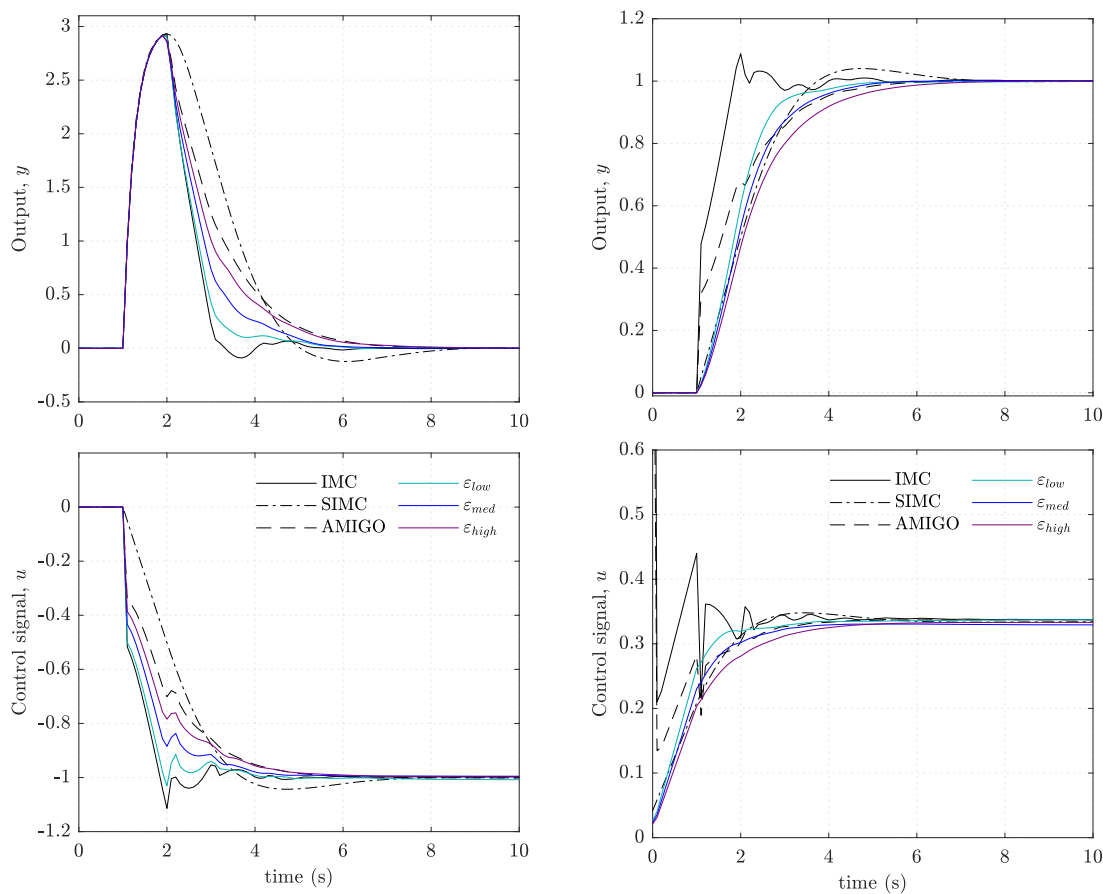


**Figure 14.** Closed loop time response of  $G_2(s)$  with the second-order LADRC tuned with the proposed rules. Comparison with the performance of ADRC<sub>Z</sub> and ADRC<sub>H</sub> controllers.



(a) Load disturbance response

(b) Set point response

**Figure 15.** Closed loop time response of  $G_2(s)$  with the second-order LADRC tuned with the proposed rules. Comparison with the performance of PID controllers.

**Table 7.** Performance comparison of proposed tuning rules with other tuning methods for control of  $G_2(s)$ . For all controllers  $M_T = 1$ . The  $\epsilon_{med}$  controller is more robust and offers a lower ITSE for disturbance rejection than the  $ADRC_Z$  controller. The three proposed alternatives offers a better disturbance rejection performance than the  $ADRC_H$  controller with similar or better robustness.

	$M_S$	$\epsilon$	Disturbance Rejection			Setpoint Following		
			ITSE	TV	$t_{98\%}$	ITSE	TV	$t_{98\%}$
IMC	1.873	2.774	15.447	1.427	3.9	0.666	2.474	3.7
SIMC	1.590	2.353	30.885	1.082	7.3	1.559	0.319	6.1
AMIGO	1.401	1.933	22.487	1.041	6.0	1.087	1.415	4.7
$ADRC_Z$	1.622	2.357	18.875	1.069	4.0	1.329	0.310	4.3
$ADRC_H$	1.792	2.612	20.278	1.361	7.6	2.122	0.310	7.3
$\epsilon_{low}$	1.798	2.615	15.817	1.321	4.9	1.381	0.312	4.1
$\epsilon_{med}$	1.638	2.296	17.551	1.102	5.3	1.550	0.308	4.7
$\epsilon_{high}$	1.526	2.073	19.930	1.038	6.1	1.775	0.312	5.5

### 7. Control of a Peltier Thermoelectric Module

The proposed tuning rules were used to design a second-order LADRC for the control of a thermoelectric module operating on the Peltier principle. It is assumed that the real behavior of the Peltier cell is modeled by the nonlinear differential equations presented in [35].

The thermal balance in the cold face is described by

$$\begin{aligned}
 Q_{cf} &= 9.2\dot{T}_c \\
 Q_{cf} &= Q_{acf} - Q_{pcf} - Q_j + Q_{cond} \\
 Q_{acf} &= 11.75 - 0.5T_c \\
 Q_{pcf} &= 0.041T_cI_p \\
 Q_j &= 0.41I_p^2 \\
 I_p &= \frac{1}{0.82}[V_{in} - 0.041(T_h - T_c)] \\
 Q_{cond} &= 0.2(T_h - T_c).
 \end{aligned}
 \tag{60}$$

The thermal balance in the hot face is

$$\begin{aligned}
 Q_{hf} &= 13\dot{T}_h \\
 Q_{hf} &= Q_{rhf} + Q_{phf} + Q_j - Q_{cond} \\
 Q_{rhf} &= 9.59(T_r - T_h) \\
 Q_{phf} &= 0.041T_hI_p.
 \end{aligned}
 \tag{61}$$

And finally, the radiator equilibrium corresponds to

$$\begin{aligned}
 Q_{rf} &= 722.55\dot{T}_r \\
 Q_{rf} &= Q_{acc} - Q_{rhf} \\
 Q_{acc} &= 167.09 - 7.11T_r
 \end{aligned}
 \tag{62}$$

The controlled output is the temperature on cold face  $T_c \in [-12.0, 6.0]$  °C and the manipulated input is the applied voltage  $V_{in}$  in percentage of its range. A block diagram representing (60)–(62) is presented in Figure 16 and the corresponding description of variables is listed in Table 8.

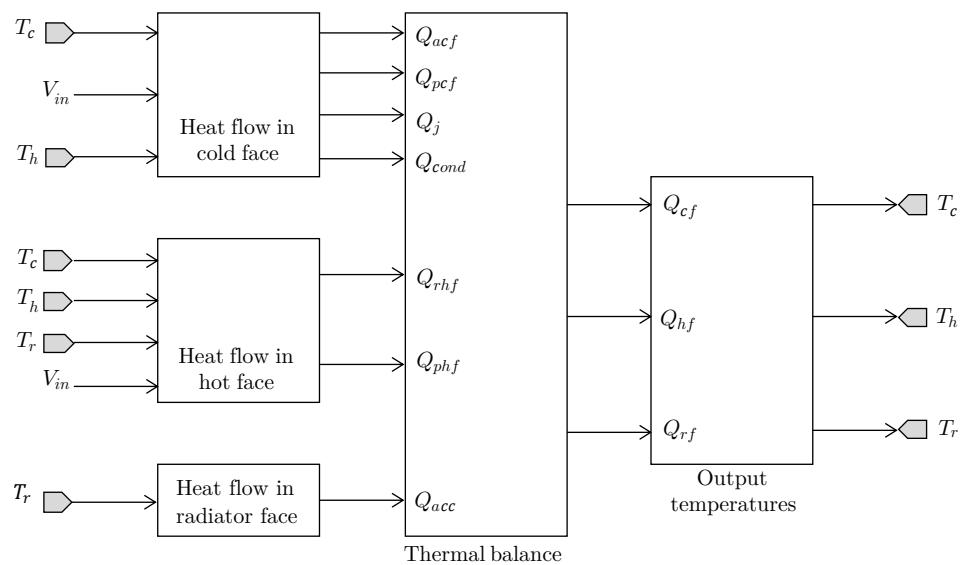


Figure 16. Block diagram of the thermoelectric module.

**Table 8.** Description of variables for the Peltier cell model.

Variable	Units	Description
$T_c$	°C	Temperature on the cold face
$T_h$	°C	Temperature on the hot face
$T_r$	°C	Temperature in the radiator
$V_{in}$	%	Voltage applied to the Peltier cell
$I_p$	A	Current flow in the Peltier cell
$Q_{cf}$	W	Net heat flow on the cold face
$Q_{acf}$	W	Heat flow transmitted by convection between the environment and the cold face
$Q_{pcf}$	W	Heat flow absorbed by the cold face due to the Peltier effect
$Q_j$	W	Heat flow generated by Peltier cell due to Joule effect
$Q_{cond}$	W	Heat flow transferred by conduction from the hot face to the cold face
$Q_{hf}$	W	Net heat flow on the hot face
$Q_{rhf}$	W	Heat flow transmitted by radiation between the hot face and radiator
$Q_{phf}$	W	Heat flow dissipated by the hot face due to Peltier effect
$Q_{rf}$	W	Net heat flow into the radiator
$Q_{acc}$	W	Heat flow transmitted by convection between the environment and the radiator

The Peltier cell behavior in the freeze zone ( $\approx -8.0$  °C) can be approximated by the FOPDT nominal model [36]

$$G_p(s) = \frac{-0.315}{3.192s + 1} e^{-0.4s}. \tag{63}$$

The normalized delay for (63) is  $\tau = 0.11$ . By substituting this value in the corresponding tuning rules, the three second-order LADRC parameters sets ( $\epsilon_{low}$ ,  $\epsilon_{med}$ ,  $\epsilon_{high}$ ) from Table 9 are obtained. Two additional controllers are also included for comparison purposes: the LADRC tuned using the proposal from [14] (ADRC<sub>Z</sub>) and a PID whose parameters were calculated by the SIMC method.

**Table 9.** Parameters for the control of a thermoelectric module.

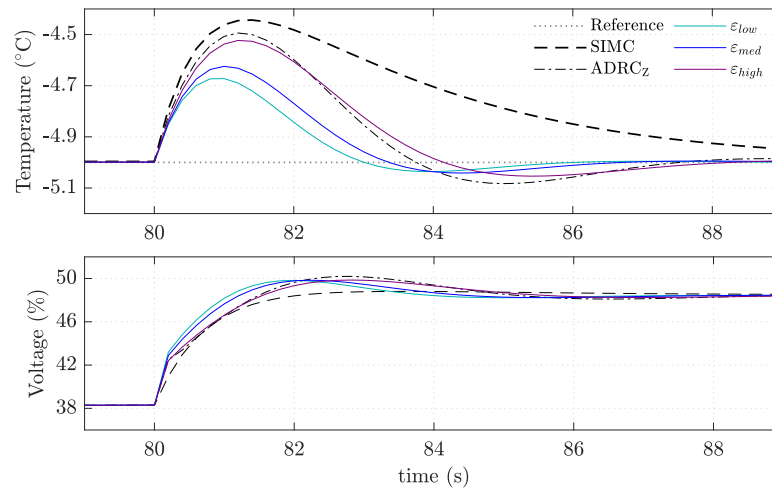
LADRC	$b_0$	$\omega_c$	$\omega_o$	PID	$K_p$	$T_i$	$T_d$
ADRC <sub>Z</sub>	-1.613	9.696	4.102	SIMC	12.667	3.192	0
$\epsilon_{low}$	-2.885	2.744	27.439				
$\epsilon_{med}$	-2.758	2.496	24.957				
$\epsilon_{high}$	-2.532	2.090	20.905				

Consider that the cold face of the module is stable at  $-5.0$  °C and a fault in power system reduces the input voltage 10% of its nominal value. The evolution of temperature  $T_c$  and the required voltage to reject the disturbance are shown in Figure 17a. The corresponding performance indices ITSE (°C<sup>2</sup> · s), TV (%) and  $t_{98\%}$ (s) are included in Table 10.

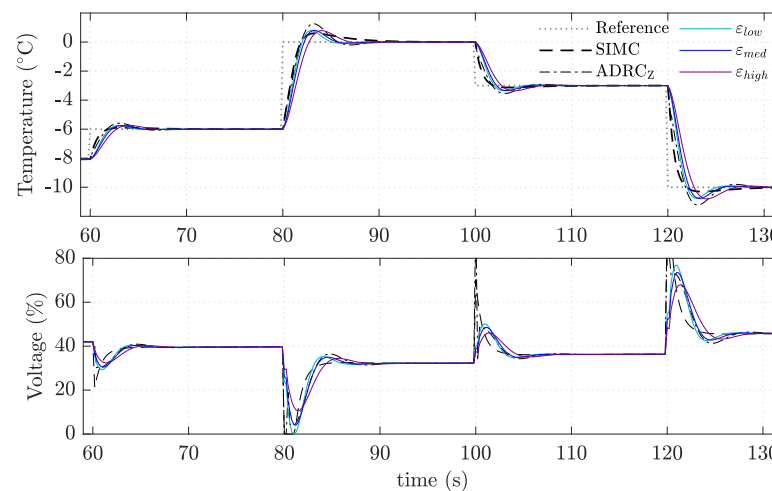
**Table 10.** Performance comparison of proposed tuning rules with reference controllers for the load disturbance response of the Peltier cell.

	$M_S$	$M_T$	$\epsilon$	ITSE	TV	$t_{98\%}$
SIMC	1.590	1.000	2.353	2.373	10.810	12.0
ADRC <sub>Z</sub>	1.545	1.455	2.607	0.773	14.001	7.0
$\epsilon_{low}$	1.848	1.516	2.721	0.188	13.121	5.0
$\epsilon_{med}$	1.749	1.425	2.511	0.302	13.152	5.8
$\epsilon_{high}$	1.613	1.298	2.232	0.725	13.173	7.2

As expected, the  $\epsilon_{low}$  controller produces the response with lower ITSE due to the relaxation in the robustness requirement. In addition, the total variation of control action and settling time are the lowest among the three proposals.



(a) Load disturbance response



(b) Setpoint following

**Figure 17.** Closed loop time response of the Peltier thermoelectric module with the second-order LADRC tuned with the proposed rules. Comparison with the performance of ADRC<sub>Z</sub> and SIMC controllers.

On the other hand, the  $\epsilon_{med}$  controller offers an improvement over the performance obtained with the ADRC<sub>Z</sub> tuning method. The robustness index is slightly lower which indicates a more robust closed loop system and the ITSE value reflects that the output stabilizes faster with less overshoot.

The most robust controller  $\epsilon_{high}$  produces a time response similar to the ADRC<sub>Z</sub> but the ITSE and TV values are slightly lower. Note that this controller also has a better disturbance rejection and robustness level than the PID tuned by the SIMC method.

The thermoelectric module can be operated at different temperatures. Due to the nonlinearities, the transient temperature response shows different behavior depending on the magnitude and direction of the setpoint changes. An additional simulation was performed to test the LADRC alternatives under this scenario.

In Figure 17b the time response of the cold face temperature with different setpoints is presented. The corresponding indices are reported in Table 11.

The three controllers designed with the proposed tuning rules guarantee the setpoint following and the steady state is reached in less time than with the other controllers. However, the ITSE values are above those calculated for the PID and ADRC<sub>Z</sub>. To clarify this behavior, the output overshoot (in % of the setpoint change) has been included in Table 11. As can be noticed, the SIMC method produces the lowest overshoot followed by the  $\varepsilon_{low}$ ,  $\varepsilon_{med}$  and  $\varepsilon_{high}$  controllers. As expected, the overshoot in output increases for high changes in the magnitude of setpoint due to the nonlinear nature of the system.

Finally, in Figure 17b it is also shown that the three design alternatives can lead to a lower variation of the control action in contrast with the abrupt change produced by the other controllers when the setpoint changes. Note that this kind of peaks may be damaging for the system. The corresponding TV indices from Table 11 support this idea.

**Table 11.** Performance comparison of proposed tuning rules and reference controllers for the setpoint response of the Peltier cell.

Setpoint (°C)	Integral of the Time Weighted Squared Error				
	SIMC	ADRC <sub>Z</sub>	$\varepsilon_{low}$	$\varepsilon_{med}$	$\varepsilon_{high}$
−8 to −6	0.766	2.361	2.253	2.772	4.027
−6 to 0	14.331	25.004	20.384	24.379	34.836
0 to −3	1.429	4.369	4.727	5.722	8.342
−3 to −10	8.026	24.814	24.757	30.629	44.931
Total Variation of Control Action					
−8 to −6	39.184	24.751	24.053	21.442	17.562
−6 to 0	32.630	71.937	59.848	53.764	43.455
0 to −3	34.185	99.566	25.580	23.286	20.042
−3 to −10	54.513	65.692	57.137	52.347	45.522
Output Overshoot					
−8 to −6	2.849	22.343	9.651	9.052	9.425
−6 to 0	7.759	23.978	10.610	11.025	10.868
0 to −3	2.255	20.693	8.061	8.722	9.152
−3 to −10	2.161	20.077	8.565	8.100	8.579
Settling Time					
−8 to −6	7.4	8.2	4.8	5.2	6.4
−6 to 0	9.2	8.2	4.8	5.4	6.6
0 to −3	7.0	8.0	4.6	5.2	6.4
−3 to −10	7.0	8.0	4.8	5.2	6.4

## 8. Conclusions

In this paper, a set of tuning rules for the second-order LADRC which offer three different levels of compromise between disturbance rejection and robustness for the control of FOPDT systems were presented. A MOOD procedure was performed to address the tuning problem. It was focused on the simultaneous minimization of the integral of time weighted squared error and a robustness measure. The tuning rules were obtained by fitting a set of Pareto optimal solutions as functions of the normalized delay and the FOPDT model parameters. Hence, all the LADRC parameters: nominal value of critical gain, controller bandwidth, and observer bandwidth can be computed by selecting a desired quality of robustness (i.e., low, medium or high) and substituting the FOPDT parameters in the given rules.

An interactive tuning software was presented as complementary material. This tool is based on the proposed rules and allows the user to adjust the LADRC parameters by varying the robustness specification between the low and high levels. On the other hand, the designer can modify the LADRC parameters within predefined intervals to evaluate the overall performance of the closed loop.

The use and convenience of the tuning rules were exemplified with the control of lag-dominated and delay-dominated systems, as well as the control of the temperature in the cold face of a thermoelectric module. The examples showed that the proposed tuning method offers satisfactory performance for load disturbance rejection and setpoint following.

As part of the conceptual framework, an overall analysis on the conflicting objectives regarding the tuning of the LADRC was done. This allows to identify as future research the possibility of expand the objective space to include other performance criteria; for example, the total variation of the control signal. The parameterization adopted in this paper for the observer bandwidth oriented the optimization process to a particular area of the stability region and as a result, smooth manipulated signals were obtained. It would be of interest to analyze the trade-offs among other design objectives.

**Author Contributions:** Conceptualization, Methodology and Writing, B.V.M. and J.S.; Review and Supervision S.G.-N. and M.M.; and Software developed, B.V.M. All authors have read and agreed to the published version of the manuscript.

**Funding:** This work was supported in part by the Ministerio de Ciencia, Innovación y Universidades, Spain, under Grant RTI2018-096904-B-I00.

**Conflicts of Interest:** The authors declare no conflict of interest.

## Abbreviations

In the following, the most important symbols and abbreviations used in this manuscript are listed.

$n$	System order
$y$	System output
$u$	Control law acting on the real plant
$a_0, a_1$	coefficients of the second-order model
$b$	Critical gain
$\bar{r}$	System setpoint
$d$	Load disturbance
$f$	Total perturbation
$b_0$	Nominal value of critical gain
$u_0$	Estate feedback control law acting on the modified plant
$x_i$	$i$ -th system real state
$z_i$	$i$ -th estimated state
$L_i$	$i$ -th observer gain
$k_i$	$i$ -th control law gain
$s$	Complex variable
$R$	Laplace transform of the system setpoint
$Y$	Laplace transform of the system output
$U$	Laplace transform of the control law
$Z_i$	Laplace transform of the $i$ -th estimated state
$G(s)$	Plant transfer function
$G_C(s)$	LADRC direct loop transfer function
$G_F(s)$	LADRC feedback transfer function
$G_A(s)$	Transfer function of controller
$G_D(s)$	Transfer function from output to load disturbance
$G_U(s)$	Transfer function to control action to output
$G_Y(s)$	Closed loop transfer function
$k$	Gain scaling of plant
$\omega_p$	Frequency scaling of plant
$\omega_o$	Observer bandwidth
$\omega_c$	Controller bandwidth
$\bar{b}_0, \bar{\omega}_c, \bar{\omega}_o$	Scaled LADRC parameters
$K$	Static gain

$T$	Apparent time constant
$l$	Apparent delay or dead time
$\Theta$	Nominal delay or dead time
$\tau$	Normalized delay or dead time
$J_1(\theta), J_2(\theta)$	Design objectives
$\theta$	Vector of decision variables
ITSE	Integral of Time Weighted Squared Error
TV	Total Variation of control action
$t_{98\%}$	Settling time
$M_s$	Maximum sensitivity
$M_T$	Complementary sensitivity
$\varepsilon$	Mixed robustness measure
$K_p, T_i, T_d$	PID controller parameters
$\varepsilon_{\text{low}}, \varepsilon_{\text{med}}, \varepsilon_{\text{high}}$	Low, medium, and high levels of robustness
$k_b, n_b, a_b, b_b, c_b$	Coefficients of the tuning rules for the nominal value of critical gain
$k_\omega, n_\omega$	Coefficients of the tuning rule for the controller and observer bandwidth

## References

- Han, J. From PID to Active Disturbance Rejection Control. *IEEE Trans. Ind. Electron.* **2009**, *56*, 900–906. [CrossRef]
- Herbst, G. A Simulative Study on Active Disturbance Rejection Control (ADRC) as a Control Tool for Practitioners. *Electronics* **2013**, *2*, 246–279. [CrossRef]
- Zheng, Q.; Gao, Z. Active disturbance rejection control: Some recent experimental and industrial case studies. *Control Theory Technol.* **2018**, *16*, 301–313. [CrossRef]
- Gao, Z. Scaling and bandwidth-parameterization based controller tuning. In Proceedings of the 2003 American Control Conference, Denver, CO, USA, 4–6 June 2003; pp. 4989–4996. [CrossRef]
- Zhao, C.; Li, D. Control design for the SISO system with the unknown order and the unknown relative degree. *ISA Trans.* **2014**, *53*, 858–872. [CrossRef]
- Sun, L.; Zhang, Y.; Li, D.; Lee, K.Y. Tuning of Active Disturbance Rejection Control with application to power plant furnace regulation. *Control Eng. Pract.* **2019**, *92*, 104122. [CrossRef]
- Zhou, R.; Tan, W. Analysis and Tuning of General Linear Active Disturbance Rejection Controllers. *IEEE Trans. Ind. Electron.* **2019**, *66*, 5497–5507. [CrossRef]
- Tan, W.; Fu, C. Linear Active Disturbance-Rejection Control: Analysis and Tuning via IMC. *IEEE Trans. Ind. Electron.* **2016**, *63*, 2350–2359. [CrossRef]
- Ahi, B.; Haeri, M. Linear Active Disturbance Rejection Control From the Practical Aspects. *IEEE/ASME Trans. Mechatron.* **2018**, *23*, 2909–2919. [CrossRef]
- Madonski, R.; Gao, Z.; Lakomy, K. Towards a turnkey solution of industrial control under the active disturbance rejection paradigm. In Proceedings of the 2015 54th Annual Conference of the Society of Instrument and Control Engineers of Japan (SICE), Hangzhou, China, 28–30 July 2015. [CrossRef]
- He, T.; Wu, Z.; Li, D.; Wang, J. A Tuning Method of Active Disturbance Rejection Control for a Class of High-Order Processes. *IEEE Trans. Ind. Electron.* **2020**, *67*, 3191–3201. [CrossRef]
- Li, D.; Chen, X.; Zhang, J.; Jin, Q. On Parameter Stability Region of LADRC for Time-Delay Analysis with a Coupled Tank Application. *Processes* **2020**, *8*, 223. [CrossRef]
- Muresan, C.I.; Birs, I.R.; Dulf, E.H. Event-Based Implementation of Fractional Order IMC Controllers for Simple FOPDT Processes. *Mathematics* **2020**, *8*, 1378. [CrossRef]
- Zhang, B.; Tan, W.; Li, J. Tuning of linear active disturbance rejection controller with robustness specification. *ISA Trans.* **2019**, *85*, 237–246. [CrossRef] [PubMed]
- Sun, L.; Hua, Q.; Shen, J.; Xue, Y.; Li, D.; Lee, K.Y. Multi-objective optimization for advanced superheater steam temperature control in a 300 MW power plant. *Appl. Energy* **2017**, *208*, 592–606. [CrossRef]
- Srikanth, M.; Yadaiah, N. Optimal parameter tuning of Modified Active Disturbance Rejection Control for unstable time-delay systems using an AHP combined Multi-Objective Quasi-Oppositional Jaya Algorithm. *Appl. Soft Comput.* **2020**, *86*, 105881. [CrossRef]
- Sun, L.; Li, D.; Gao, Z.; Yang, Z.; Zhao, S. Combined feedforward and model-assisted active disturbance rejection control for non-minimum phase system. *ISA Trans.* **2016**, *64*, 24–33. [CrossRef]
- Martínez, B.V. LADRC Automatic Parameters Computation Based on Robustness. Version 1.0.0. 2021. Available online: <https://es.mathworks.com/matlabcentral/fileexchange/86403> (accessed on 26 January 2021).
- Zheng, Q.; Gao, L.Q.; Gao, Z. On Validation of Extended State Observer Through Analysis and Experimentation. *J. Dyn. Syst. Meas. Control* **2012**, *134*. [CrossRef]
- Zhao, S.; Gao, Z. Modified active disturbance rejection control for time-delay systems. *ISA Trans.* **2014**, *53*, 882–888. [CrossRef]

21. Visioli, A. Identification and Model Reduction Techniques. In *Practical PID Control-Advances in Industrial Control*; Grimble, M.J., Johnson, M.A., Eds.; Springer: London, UK, 2006; pp. 165–207.
22. Reynoso-Meza, G.; Blasco-Ferragud, X.; Sanchis-Saez, J.; Herrero-Durá, J.M. Background on Multiobjective Optimization for Controller Tuning. In *Controller Tuning with Evolutionary Multiobjective Optimization. Intelligent Systems, Control and Automation: Science and Engineering*; Tzafestas, S.G., Ed.; Springer: Cham, Switzerland, 2017; Volume 85, pp. 23–58. [[CrossRef](#)]
23. Skogestad, S.; Postlethwaite, I. Classical Feedback Control. In *Multivariable Feedback Control-Analysis and Design*; John Wiley and Sons: Hoboken, NJ, USA, 2001; pp. 15–62.
24. Tan, W.; Liu, J.; Chen, T.; Marquez, H.J. Comparison of some well-known PID tuning formulas. *Comput. Chem. Eng.* **2006**, *30*, 1416–1423. [[CrossRef](#)]
25. Åström, K.J.; Hägglund, T. Process models. In *Pid Controllers: Theory, Design and Tuning*; Instrument Society of America: Pittsburgh, PA, USA, 1995; pp. 5–58.
26. Garpinger, O.; Hägglund, T.; Åström, K.J. Performance and robustness trade-offs in PID control. *J. Process Control* **2014**, *24*, 568–577. [[CrossRef](#)]
27. Lee, Y.; Park, S.; Lee, M.; Brosilow, C. PID controller tuning for desired closed-loop responses for SI/SO systems. *AIChE J.* **1998**, *44*, 106–115. [[CrossRef](#)]
28. Skogestad, S.; Grimholt, C. The SIMC Method for Smooth PID Controller Tuning. In *PID Control in the Third Millennium*; Vilanova, A.V.R., Ed.; Springer: Berlin/Heidelberg, Germany, 2012; pp. 147–175. [[CrossRef](#)]
29. Åström, K.; Hägglund, T. Revisiting the Ziegler–Nichols step response method for PID control. *J. Process Control* **2004**, *14*, 635–650. [[CrossRef](#)]
30. Reynoso-Meza, G.; Sanchis, J.; Blasco, X.; Herrero, J.M. Multiobjective evolutionary algorithms for multivariable PI controller design. *Expert Syst. Appl.* **2012**, *39*, 7895–7907. [[CrossRef](#)]
31. Herrero, J.M.; Martínez, M.; Sanchis, J.; Blasco, X. Well-Distributed Pareto Front by Using the  $\epsilon^{\lambda}$ -MOGA Evolutionary Algorithm. In *Computational and Ambient Intelligence*; Sandoval, F., Prieto, A., Cabestany, J., Graña, M., Eds.; Springer: Berlin/Heidelberg, Germany, 2007; pp. 292–299. [[CrossRef](#)]
32. Méndez, M.; Frutos, M.; Miguel, F.; Aguasca-Colomo, R. TOPSIS Decision on Approximate Pareto Fronts by Using Evolutionary Algorithms: Application to an Engineering Design Problem. *Mathematics* **2020**, *8*, 2072. [[CrossRef](#)]
33. Cuate, O.; Schütze, O. Pareto Explorer for Finding the Knee for Many Objective Optimization Problems. *Mathematics* **2020**, *8*, 1651. [[CrossRef](#)]
34. Sánchez, H.S.; Visioli, A.; Vilanova, R. Optimal Nash tuning rules for robust PID controllers. *J. Frankl. Inst.* **2017**, *354*, 3945–3970. [[CrossRef](#)]
35. Huilcapi, V.; Herrero, J.M.; Blasco, X.; Martínez-Iranzo, M. Non-linear identification of a Peltier cell model using evolutionary multi-objective optimization. *IFAC-PapersOnLine* **2017**, *50*, 4448–4453. [[CrossRef](#)]
36. Reynoso-Meza, G.; Blasco-Ferragud, X.; Sanchis-Saez, J.; Herrero-Durá, J.M. Multiobjective Optimization Design Procedure for Controller Tuning of a Peltier Cell Process. In *Controller Tuning with Evolutionary Multiobjective Optimization. Intelligent Systems, Control and Automation: Science and Engineering*; Tzafestas, S.G., Ed.; Springer: Cham, Switzerland, 2017; Volume 85, pp. 187–199. [[CrossRef](#)]